# Investigating Volatile Organic Compound Emissions from Boreal Lake Water Exposed to Ultraviolet Light and Ozone

Hanne Ødegaard Notø

Thesis for the Master's degree in Chemistry
Environmental Chemistry
60 credits

Department of Chemistry
Faculty of Mathematics and Natural Sciences

UNIVERSITY OF OSLO

June 2021

# Investigating Volatile Organic Compound Emissions from Boreal Lake Water Exposed to Ultraviolet Light and Ozone

**Hanne Ødegaard Notø**

Thesis for the Master's degree in Chemistry

60 credits

Department of Chemistry

Faculty of Mathematics and Natural Sciences

University of Oslo

June 2021

2021

Investigating Volatile Organic Compound Emissions from Boreal Lake Water Exposed to Ultraviolet Light and Ozone

Hanne Ødegaard Notø

http://www.duo.uio.no/

Trykk: Reprosentralen, Universitetet i Oslo

# Abstract

Inland surface waters are an important part of the global carbon cycle through sedimentation, atmospheric emissions, dissolution of atmospheric carbon dioxide ($CO_2$) and the transport of dissolved carbon in runoff. The surface microlayer (SML) is a thin film on the surface of waters consisting of fatty acids, lipids and other organic compounds which serve as the interface between the hydrosphere and atmosphere. The organic compounds in the SML can photooxidize and constitute a source of reactive organic compounds that contribute to the formation of tropospheric ozone ($O_3$) and secondary organic aerosols, consequently affecting air quality and climate. This study investigated the volatile organic compound (VOC) emissions from ten boreal lake water samples exposed to ultraviolet (UV) light and atmospheric $O_3$. The aim was to study the drivers of VOC emissions and examine if the main source of the emissions was the SML or subsurface water. High emissions of methanol, acetaldehyde, acetone/propanal, hexanal and nonanal were observed. UV light was the main driver of these emissions, and high UV intensities produced higher amounts of VOCs. Emissions of acetone/propanal and pentanal were formed by $O_3$ exposure in one of the lakes studied. There was a correlation between the total organic carbon concentration and the VOC emission levels. The SML did not contribute to higher emissions than the subsurface water.

# Preface

The present work was carried out at the Department of Chemistry at the University of Oslo (UiO) from August 2019 to June 2021. Part of the experimental work was performed at the Department of Biosciences, UiO. My supervisors have been professor Armin Wisthaler, professor Dag Olav Hessen and professor Rolf D. Vogt.

First and foremost, I would like to thank my supervisor Armin Wisthaler for support and guidance throughout this process. A big thanks to Felix Piel for helping me with the instrument and giving valuable feedback during the writing process. Thank you to Tomas Mikoviny for giving me training on the PTR-MS and help with the instrument. I would also like to thank my co-supervisor Dag O. Hessen for the encouragement, especially during the last months of writing. Thank you to my co-supervisor Rolf D. Vogt for always keeping an open door and providing advice. Thank you to Alexander Eiler for letting me join his field trip to collect my samples, to Per-Johan Færøvig for introducing me to Q-SUN, and to Berit Kaasa for analyzing my samples with the TOC analyzer.

Thank you to all the incredible people in the Environmental Chemistry group. A special thanks goes to Elisabeth Syse, Markus Sørensen, Baptiste Languille, Alexander Håland, Anjitha Sarachandra Kumar Geetha, Ragna Othilie Lie and Susanne Jøntvedt Jørgensen. I appreciate the great conversations and discussions we have had, and I am grateful for the positive social and academic environment in this group.

Finally, I would like to thank my parents and sisters for supporting me through this entire process. This work could not have been done without your love and encouragement.

Oslo, Norway, June 2021

Hanne Ødegaard Notø

# Table of Contents

# 1 Introduction

Inland surface waters are an integral part of the global carbon cycle through the transport of dissolved carbon in runoff, sedimentation, atmospheric emissions and dissolution of atmospheric carbon dioxide ($CO_2$). Drake and co-workers estimated that inland waters receive more than 5.1 Pg C $yr^{-1}$ from terrestrial landscapes (Drake, Raymond, and Spencer 2018). Dean and co-workers found that lakes, peatlands and sedimentation in fresh water are a greater sink for organic carbon than the oceans, which is due to major inputs of terrestrial organic carbon (Dean 1998). Inland surface waters are, however, also a significant source of atmospheric carbon. Drake and co-workers estimated that about 3.9 Pg C $yr^{-1}$ is transferred to the atmosphere through outgassing (Drake, Raymond, and Spencer 2018). Previous work has focused on carbon emissions in the form of greenhouse gases, $CO_2$ and methane ($CH_4$), which are formed through chemical and biological degradation of organic matter (Tranvik et al. 2009). Such emissions are driven by biotic processes (mainly microbial) and photooxidation occuring in the surface layers due to high attenuation of shortwave radiation caused by chromophoric dissolved organic carbon(Thrane, Hessen, and Andersen 2014; Allesson et al. 2021). Photooxidation of natural organic matter is, however, also known to form highly reactive and poorly soluble organic molecules such as small aldehydes (Anglada et al. 2020; Rossignol et al. 2016; Fu et al. 2015). Once escaped to the atmosphere, these reactive organic compounds play a major role in atmospheric chemistry, contributing to the formation of tropospheric ozone ($O_3$) and secondary organic aerosols (SOA) and thereby affecting air quality and climate (Bernard et al. 2016). The formation and emission of reactive organic trace gases has been studied previously for the marine surface microlayer (SML), i.e. the thin film at the interface between the ocean and the atmosphere, which has a high content of fatty acids and lipids and is enriched in dissolved natural organic matter (DNOM), nutrients, trace metals, phytoplankton, and bacteria relative to subsurface water (Wurl et al. 2017; Knulst et al. 1997; Ebling and Landing 2015; Cuong, Karuppiah, and Obbard 2008; Zhang et al. 2003; Tovar-Sánchez, González-Ortegón, and Duarte 2019; Zäncker et al. 2017; Martinez-Varela et al. 2020). The SML is directly exposed to sunlight and is in direct contact with the atmosphere, including the oxidants OH radicals and ozone ($O_3$). Studies done on photooxidation of the SML have shown that unsaturated fatty acids photooxidize to form saturated aldehydes (Kieber, Hydro, and Seaton 1997; Ciuraru et al. 2015). Fatty acids comprise about 3% of the total DNOM in seawater (Kattner, Gercken, and Hammer 1983). Chiu and co-workers proposed the following

mechanism for the photooxidation of carboxylic acids in the air-water interface (Chiu et al. 2017):

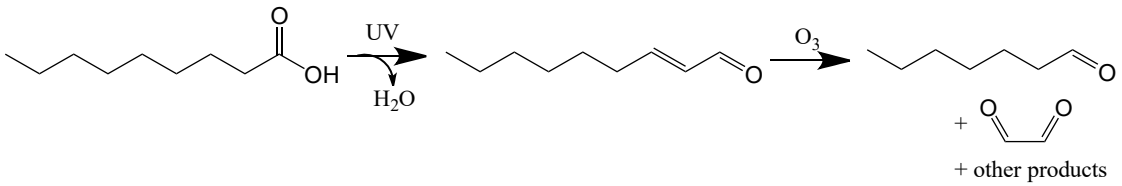


Figure 1. Suggested mechanism for photooxidation of carboxylic acids. In the first step, carboxylic acid is transformed into an unsaturated aldehyde. In the second step, the unsaturated aldehyde undergoes ozonolysis and is cleaved into a saturated aldehyde and glyoxal among other products. Adapted from Chiu et al. (2017)

The photooxidation of carboxylic acids in the presence of $O_3$ thus leads to the formation of saturated aldehydes and glyoxal. This study was performed in a laboratory setting, but field studies support the production of saturated aldehydes from photooxidation(Carpenter, Archer, and Beale 2012). Zhou and Mopper found strong diurnal variations in the concentrations of formaldehyde, acetaldehyde, propanal, glyoxal, methylglyoxal, glyoxylic acid and pyruvic acid in the SML of sea water samples, with maxima in the early afternoon and a minima in the early morning (Zhou and Mopper 1997). They also found an enrichment of these compounds in the SML compared to the bulk sea water, and this enrichment was higher after exposing the samples to sunlight. This suggests that the photoproduction of the LMW carbonyl compounds in the SML is higher than in the bulk samples. Fu and co-workers studied the formation of aldehydes and carboxylic acids from alcohols in the presence of photosensitizers (Fu et al. 2015). They proposed the following mechanisms occurring in the SML and in the bulk water:

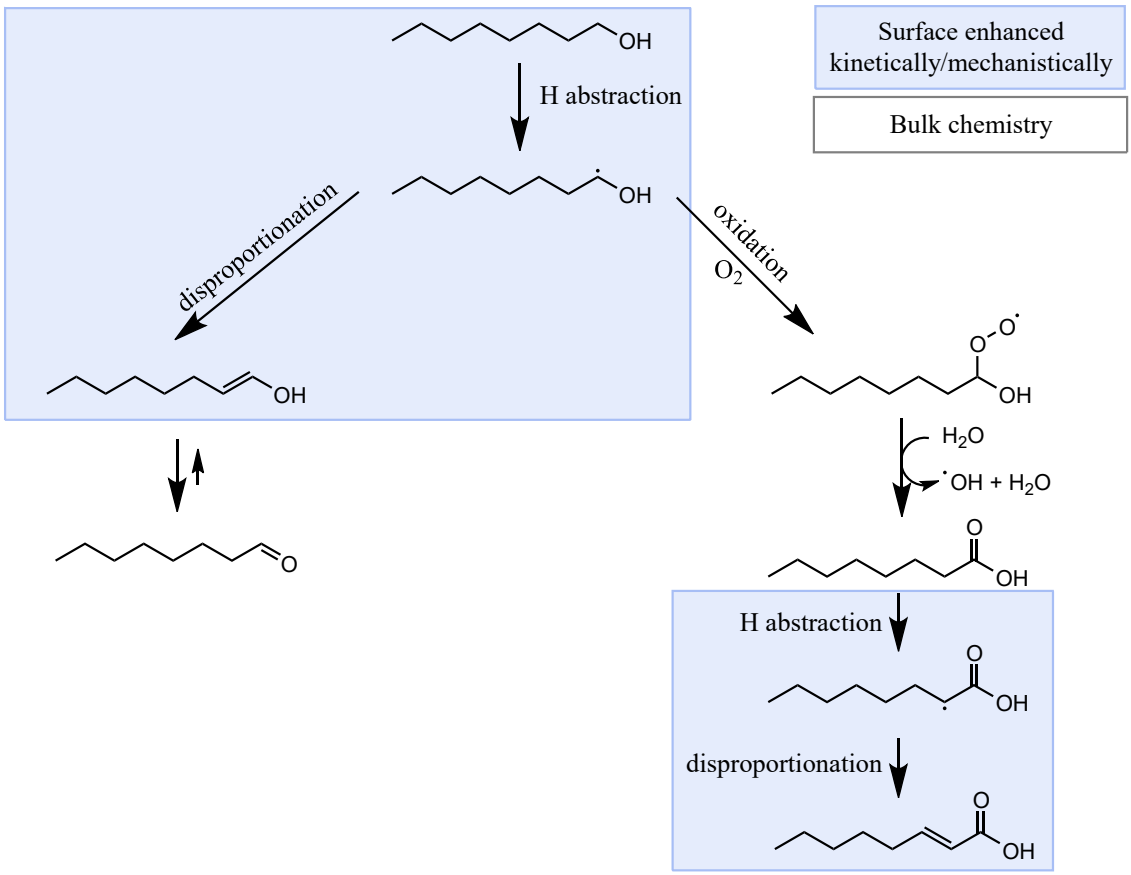


Figure 2. Suggested mechanism for photochemical reactions at the air-sea water interface in the presence of octanol and a photosensitizer. Adapted from Fu et al. (2015).

The work of Bertilssson and co-workers supports the photochemical production of carboxylic acids in river samles (Bertilsson et al. 1999).

Seco and co-workers measured the flux of organic trace gases from lake Villasjön in Sweden and found that the lake was a net sink for acetone and acetaldehyde (Seco et al. 2020). They also found emissions of methanol and isoprene, although there was no net flux measured between the atmosphere and the lake. A fen near the lake exhibited a flux of methanol, acetone, and isoprene into the atmosphere during the day. Emissions were stronger in July than in September suggesting that these species were formed though photooxidation.

While photooxidation has been in the focus of research, a few studies investigated ozonolysis of fatty acids as the source of reactive organic trace gases. Zhou and co-workers proposed a mechanism forming aldehydes from the ozonolysis of polyunsaturated fatty acids in the SML (Figure 3) (Zhou et al. 2014).

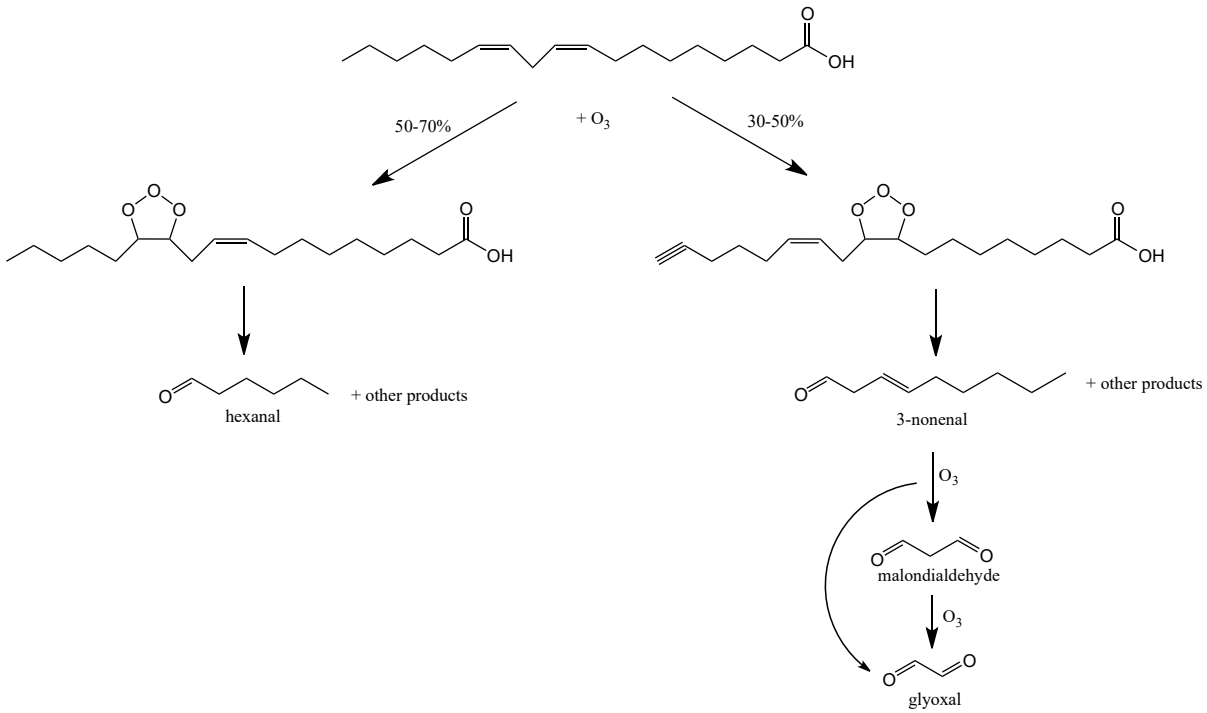


Figure 3. Proposed mechanism for ozonolysis of a polyunsaturated carboxylic acid (linoleic acid) into aldehydes and dialdehydes among other products, occurring in the air-sea water interface. Adapted from Zhou et al. (2014)

To the best of the author's knowledge, no studies have hitherto investigated the emissions of reactive organic trace gases from the SML of lake water. Lake water has the potential to produce higher organic trace gas emissions than the oceans since lakes typically have much higher concentrations of organic matter. Hence it is surprising that no research has been done on this area. The aim of this study was to characterize and quantify the emissions of reactive organic trace gases from lake water samples upon exposure to UV light and $O_3$. Understanding the driver of the emissions was of key interest, in addition to determining if the main source of the emissions was the surface microlayer or the bulk water. The hypothesis was that the SML samples being enriched in organic material would produce higher emissions than the bulk water samples. Exposure to UV radiation was expected to produce higher emissions than ozonolysis, because light penetrates the water while ozone only reacts at the air-water interface. The samples from different lakes were hypothesized to have different emission rates because of differences in their total organic carbon (TOC) content, assuming that the TOC content scales with the concentrations of degradable carbon.

# 2 Methods

## 2.1 Investigated lakes

In the frame of this Master project, I investigated water samples from ten boreal lakes located in southeastern Norway. The chosen lakes show substantial variation in their physicochemical properties, which include organic matter content, salt level, pH and color as well as trophic states ranging from oligotrophic (nutrient limited systems) to eutrophic (nutrient rich waters) (for details, see Table 4 in Appendix A1). The lake surface areas span from $4.6\times10^{-3}$ to 2.6 $km^2$, and the catchment areas range from 0.29 to 81 $km^2$(Noregs vassdrags- og energidirektorat (NVE) 2020). Details are given in Table 1 below. In total, I collected 10 bulk water and 9 surface microlayer samples between October 21 and November 5, 2020.

Table 1. Geographical information on the sampled lakes. The data is obtained from the Norwegian Water Resources and Energy Directorate's lake database(Noregs vassdrags- og energidirektorat (NVE) 2020).

| Lake | Elevation (m) | Surface area ($km^2$) | Catchment area ($km^2$) |
|---|---|---|---|
| Gjersjøen | 40 | 2.7 | 82 |
| Kolbotntjern | 95 | 0.29 | 3.1 |
| Lutvann | 205 | 0.42 | 1.7 |
| Tennungen | 298 | 0.28 | 8.6 |
| Tjernsrudtjern | 61 | 0.011 | 0.65 |
| Sessvoldtjern | 200 | 0.018 | 1.3 |
| Svartkulp | 372 | 0.0046 | 0.29 |
| Sværsvann | 136 | 0.48 | 16 |
| Østensjøvann | 107 | 0.33 | 12 |
| Årungen | 34 | 1.2 | 50 |

## 2.2 Sampling, filtration, storage and preparation for use

The bulk water samples were collected 30-50 cm from the shore directly in 1 L amber glass bottles from each of the 10 lakes included in the study. The water was sampled 0-5 cm below the water surface and the total volume of water collected from each lake was 1-7 L. The surface microlayer (SML) of the lakes was sampled according to the procedure described by Harvey and Burzell (1972). The sampling is based on the principle that the lipophilic surface layer adheres to a plastic plate to a higher degree than the hydrophilic bulk water. The sampling plate used was a 5 mm thick acrylic sheet with a handle attached to the short end of the 40×50 cm

plate. The effective sampling surface area of the plate was 40×45 cm as some of the plate was cut out to make the handle. Figure 4 below depicts the sampling plate in use. To collect the sample, the plate was held by the handle and dipped vertically into the water before being withdrawn from the water at a rate of approximately 5-10 cm $s^{-1}$. The surface microlayer and water adhering to the plate was then removed from both sides with a rubber squeegee and collected in a wide glass beaker before being transferred to amber glass bottles.

Figure 4. Sampling of the surface microlayer using the sampling plate.

All samples were stored in a dark refrigerated room at 4°C until analysis to decelerate chemical and biological degradation in the samples between sampling and analysis.

For testing the potential biological sample degradation and its effect on VOC emissions, water from the Svartkulp lake was split into three parts. One part was left unfiltered, the second part was filtered through a 0.45 µm filter (Merck Millipore, Burlington, Massachusetts, United States), and the third part was filtered through a 0.2 µm filter (Merck Millipore, Burlington, Massachusetts, United States). The samples from Svartkulp lake were chosen for this experiment because it had the highest sample volume. The filtration took place 0-2 days after the sample was collected and a vacuum filtration system was used. The filters were primed and

flushed with type I water to remove loose filter material prior to introducing the sample. Filtering through a 0.45 µm filter is expected to remove a major part of the bacteria plus all phytoplankton and is commonly used for separating the particulate and dissolved fractions of the water. Filtering through a 0.2 µm filter is expected to remove all bacteria, thus leaving behind a (semi)sterile sample. The filtered samples were stored and analyzed like the rest of the samples.

Before analysis, a 200 mL aliquot from the refrigerated sample was transferred to a measuring cylinder and added to the vessel used for conducting the experiments (see section 3.2).

## 2.3 Photooxidation set-up

To study water-atmosphere interactions, I conducted three different types of experiments. Water samples were exposed to either: i) UV-light, ii) ozone ($O_3$) or iii) UV-light + $O_3$. These conditions were chosen to simulate natural conditions and observe the effects of UV radiation and $O_3$ on DNOM in lakes, both separately and cumulatively. All samples were left untreated, with the exception of part of the sample from Svartkulp, to keep the laboratory conditions as close as possible to natural conditions. For this reason the UV radiation and $O_3$ concentrations were kept at levels which can be expected in the natural environment.

In the UV condition, samples were irradiated with artificial sunlight produced by a Q-SUN Xe-1 (Q-Panel Lab Products, Cleveland, Ohio, United States) device. The irradiance of the Q-SUN is 0.68 W $m^{-2}$ at 340 nm and the radiation is in the range between 300 and 800 nm, mimicking natural solar radiation. Figure 5 below compares the irradiance of the Q-SUN with daylight filter and natural sunlight in the wavelength range between 200 and 800 nm.

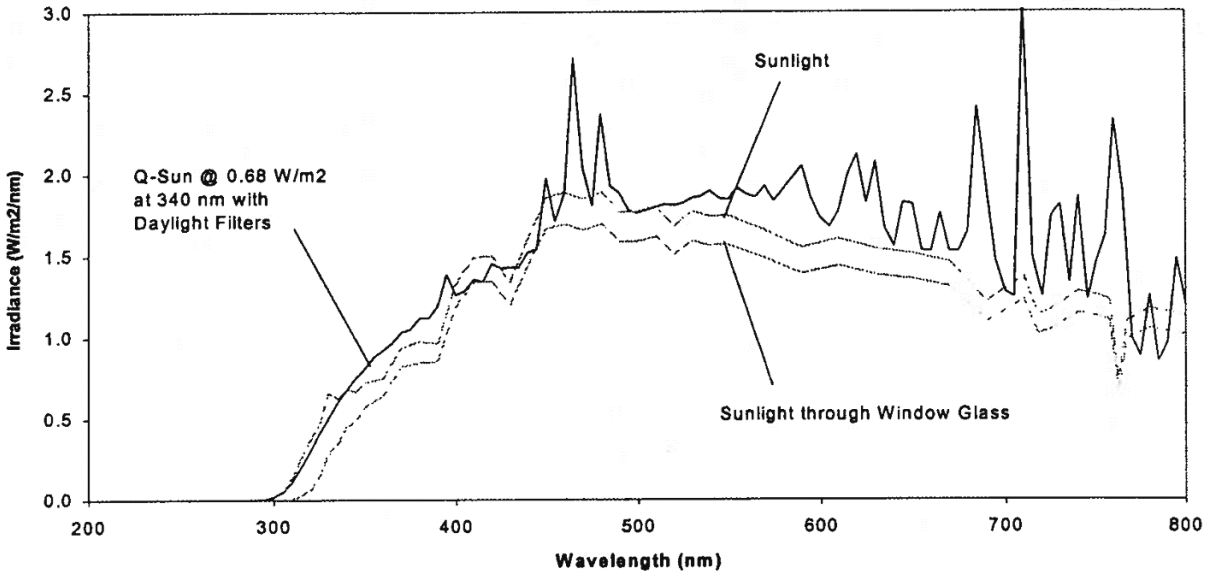


Figure 5. Comparison of the irradiance of the Q-SUN with daylight filter vs. sunlight at 200-800 nm. Obtained from Q-SUN Xenon Test Chamber Operating Manual (Q-Panel Lab Products, 2002).

In the $O_3$ condition, 40 ppb $O_3$ produced by a UVP Stable Ozone Generator (Analytik Jena GmbH, Jena, Germany) was introduced into the sample gas flow. The 40 ppb level was chosen because it is within the normal range of tropospheric $O_3$ levels during summer in Scandinavia(Schultz et al. 2017). The $O_3$ generator consisted of a quartz tube positioned next to a short wavelength UV lamp. UV radiation at 185 nm photolyzes $O_2$ in the air flowing through the quartz tube, thereby producing a continuous flow of air containing $O_3$. In condition iii), the sample was simultaneously exposed to UV radiation and $O_3$. Exposure of the samples lasted from 4 and 180 minutes, and samples from the same lake were exposed for roughly the same amount of time.

Figure 6 shows a scheme of the experimental set-up. An in-house built zero air generator (including a platinum-palladium catalyst) was used to create a steady 2.8 slpm supply of VOC-free and $O_3$-free air. The zero air then passed through the $O_3$ generator before being divided between the $O_3$ analyzer (1.6 slpm) and the exposure set-up. The PTR-MS instrument pulled a flow of 370 sccm through the sample vessel, while the overflow was discarded. A relatively high flow through the sample vessel was used to minimize the residence time and gas-phase reactions in the sample headspace. The sampling tubes that were exposed to UV light were shielded with aluminum foil to prevent any UV-catalyzed reactions outside the sample vessel. The sampling line of the PTR-MS instrument was heated to 80°C to prevent condensation. Figure 7 below shows a photo of the experimental set-up in the laboratory.

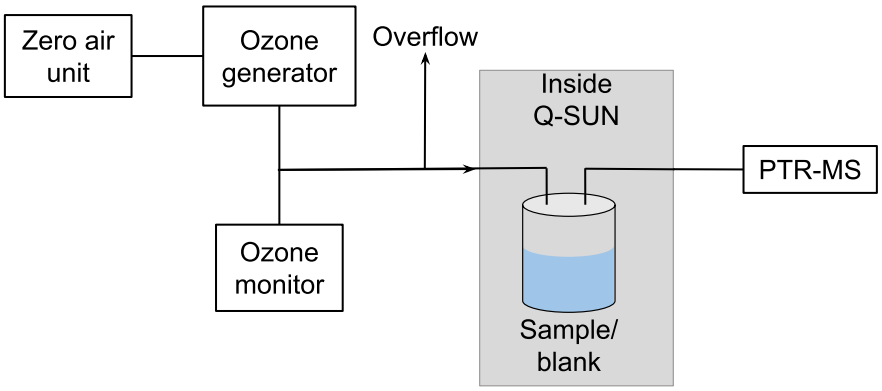


Figure 6. Schematic of the experimental set-up.

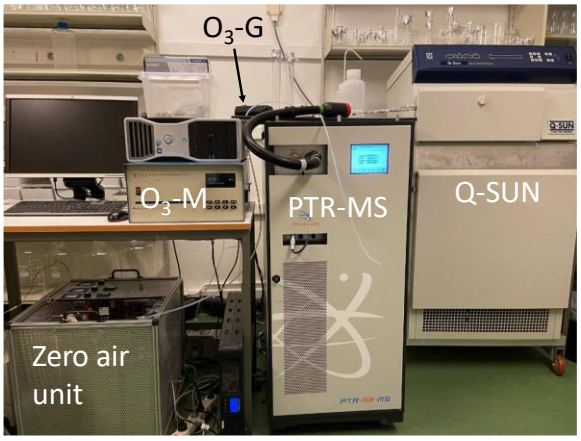


Figure 7. Photo of the instrument set-up in the laboratory, including the zero air unit, ozone generator ($O_3$-G), ozone monitor ($O_3$-M), Q-SUN and PTR-MS instrument.

The sample vessel was a custom-made 500 mL glass beaker with a quartz lid (see Figure 8). The lid had two quartz ports (inlet/outlet) and quartz was chosen because it is UV transparent, while conventional glass is not. A Teflon/PTFE seal was placed between the beaker and the lid and fixed with round screw clamp for keeping the sample vessel sealed during the experiment.

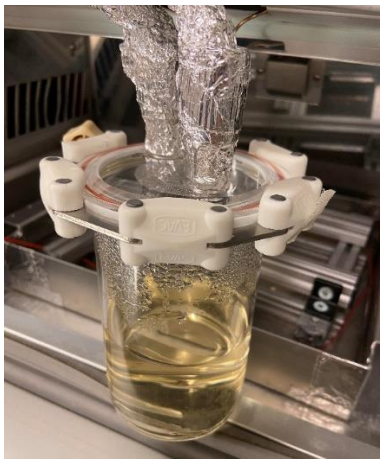

Figure 8. Sample vessel.

The water sample was transferred into the sample vessel as described in section 2.2. The vessel was then sealed and the sample was left to stabilize for 3-15 minutes before the exposure started. Samples were only used for one condition before being discarded.

Before analyzing lake samples, a blank measurement was conducted using HPLC grade water (VWR International, Radnor, Pennsylvania, United States).

## 2.4 Proton-transfer-reaction mass spectrometer measurements and data analysis

Proton-transfer-reaction mass spectrometry (PTR-MS) is a mass spectrometric method, which involves chemical ionization of gaseous analytes (A) via hydronium ions ($H_3O^+$) through the following reaction(Hansel et al. 1995):

$$H_3O^+ + A \rightarrow AH^+ + H_2O \quad (1)$$

The proton transfer reaction (1) is energetically favorable if the analyte has a higher proton affinity (PA) than $H_2O$ (691 kJ $mol^{-1}$ (Peterson et al. 1998)). Almost all VOCs have proton affinities higher than water, the only exceptions being low mass alkanes (< $C_9$) and small alkenes (< $C_3$). The main components of air, *i.e.* $N_2$, $O_2$ and Ar, have a PA lower than water and are thus not ionized upon collisions with $H_3O^+$. If the proton transfer reaction (1) is exothermic, it occurs at the collisional rate.

A proton-transfer-reaction mass spectrometer consists of three main parts: an ion source, a drift tube and a mass analyzer. Figure 9 shows a scheme of a PTR-MS instrument and its main components.

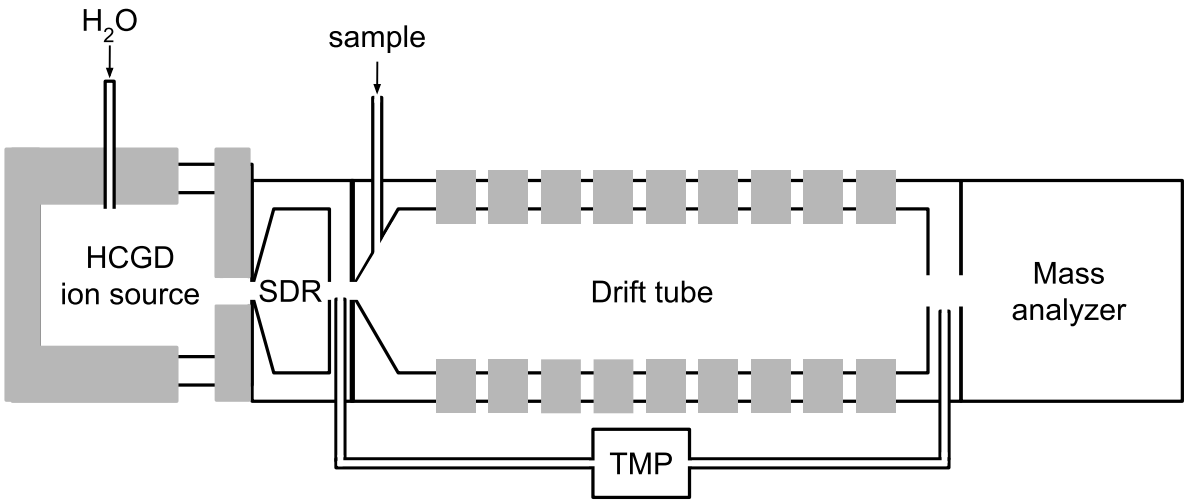


Figure 9. Diagram of the PTR-MS instrument including a hollow cathode glow discharge (HCGD) ion source, a source drift region (SDR), a drift tube (DT) and a mass analyzer. TMP: turbomolecular pump

A hollow cathode glow discharge (HCGD) ion source yields a high purity (>99%) $H_3O^+$ ion swarm by electron ionization of water vapor. In the HCGD ion source, $H_2O$ is ionized by electrons and the following reactions take place(Mann, Hustrulid, and Tate 1940):

$$H_2O + e^- \rightarrow O^+ + 2e^- + H_2 \quad (2)$$

$$H_2O + e^- \rightarrow OH^+ + 2e^- + H \quad (3)$$

$$H_2O + e^- \rightarrow H^+ + 2e^- + OH \quad (4)$$

$$H_2O + e^- \rightarrow {H_2}^+ + 2e^- + O \quad (5)$$

$$H_2O + e^- \rightarrow H_2O^+ + 2e^- \quad (6)$$

These ions are then extracted into the source drift region where they react further to form $H_3O^+$ through one or more of the following reactions:

$$O^+ + H_2O \rightarrow H_2O^+ + O \quad (7)$$

$$OH^+ + H_2O \rightarrow H_2O^+ + OH \quad (8)$$

$$OH^+ + H_2O \rightarrow H_3O^+ + O \quad (9)$$

$$H^+ + H_2O \rightarrow H_2O^+ + H \quad (10)$$

$$H_2{}^+ + H_2O \rightarrow H_3O^+ + H \quad (11)$$

$$H_2{}^+ + H_2O \rightarrow H_2O^+ + H_2 \quad (12)$$

$$H_2O^+ + H_2O \rightarrow H_3O^+ + OH \quad (13)$$

The $H_3O^+$ ions are then extracted through an orifice into the drift tube (DT), where they ionize the sample. The sample enters the DT through an inlet capillary wherein the pressure drops from atmospheric pressure to a few mbar. Ambient air is directly sampled into the DT, no sample preparation or treatment is necessary.

The DT is a cylinder consisting of 10 stainless-steel ring electrodes separated equally by polytetrafluoroethylene (PTFE) insulators. The voltage across the DT is typically in the range between 350 and 700 V and each ring electrode is kept at a different voltage to create a uniform electric field in axial direction. This field draws the ions along the DT and defines their velocity. The DT pressure is typically in the range between 2 and 4 mbar and is regulated by a pressure controller connected to the inlet capillary. The reduced electric field (E/N) is an essential parameter in PTR-MS, and it is the electric field strength (E) in the DT divided by the gas number density (N). The E/N regulates the abundance of hydronium-water clusters in the DT. The $H_2O.H_3O^+$ cluster (dimer) and $(H_2O)_2.H_3O^+$ cluster (trimer) form at low E/N. As the dimer and trimer may react differently with VOCs than $H_3O^+$, the presence of these hydrates complicates the quantitative interpretation of PTR-MS mass spectra. To limit the formation of these and even larger water clusters, the DT is typically operated at high E/N. At high E/N, the added kinetic energy from the electric field fragments the ion clusters in collisions with the background gas. The drawback of operating the DT at a high E/N is that it may increase fragmentation of the protonated VOCs due to the added kinetic energy. The E/N is given in the unit Townsend (Td) where 1 Td is $10^{-17}$ V cm². The E/N typically lies in the range between 100 and 140 Td, but it must be tuned to fit the application.

At the end of the drift tube there is a small aperture, through which the ions enter the mass spectrometer (MS). The entrance must be narrow because the pressure inside the MS ($10^{-6}$ – $10^{-7}$ mbar) is several orders of magnitude lower than in the DT.

Time-of-flight mass spectrometry (ToF-MS) is the state-of-the-art mass analysis method in PTR-MS. PTR-ToF-MS instruments include the following main parts: an acceleration region, a field free region and a detector, as shown in Figure 10. Ions exit the DT, pass through the ion transfer region and enter the acceleration region, where they are orthogonally pulsed into the field free region. This is known as orthogonal acceleration ToF-MS (oa-ToF-MS) and allows a continuous ion source to be coupled to a ToF-MS, which requires a discontinuous stream of ions. The acceleration region consists of two electrodes: a repeller plate (RP) and an extractor grid (EG). During filling of the acceleration region, repeller and extractor are at the same potential to not alter the path of the ions. For extraction into the field-free region, a few microseconds long high voltage pulse is applied to the extraction grid. This pulse diverts the ions into the field-free drift region, where they are separated based on their time of flight. The region is kept field-free by shielding the ions with a cage which is either connected to a high voltage supply or grounded. Since the ions entering the acceleration region have the same energy and are given the same energy during the acceleration pulse, the time of flight ($t$) of the individual ions is determined by:

$$t = l\sqrt{\frac{1}{2eV} \times \frac{m}{z}} \tag{14}$$

where $l$ is the flight path, $e$ is the elementary charge and $V$ is the potential difference between the repeller plate and the extraction grid. As seen here the time of flight is directly proportional to $\sqrt{m/z}$, which is why the $m/z$ of the ions can be obtained with this method.

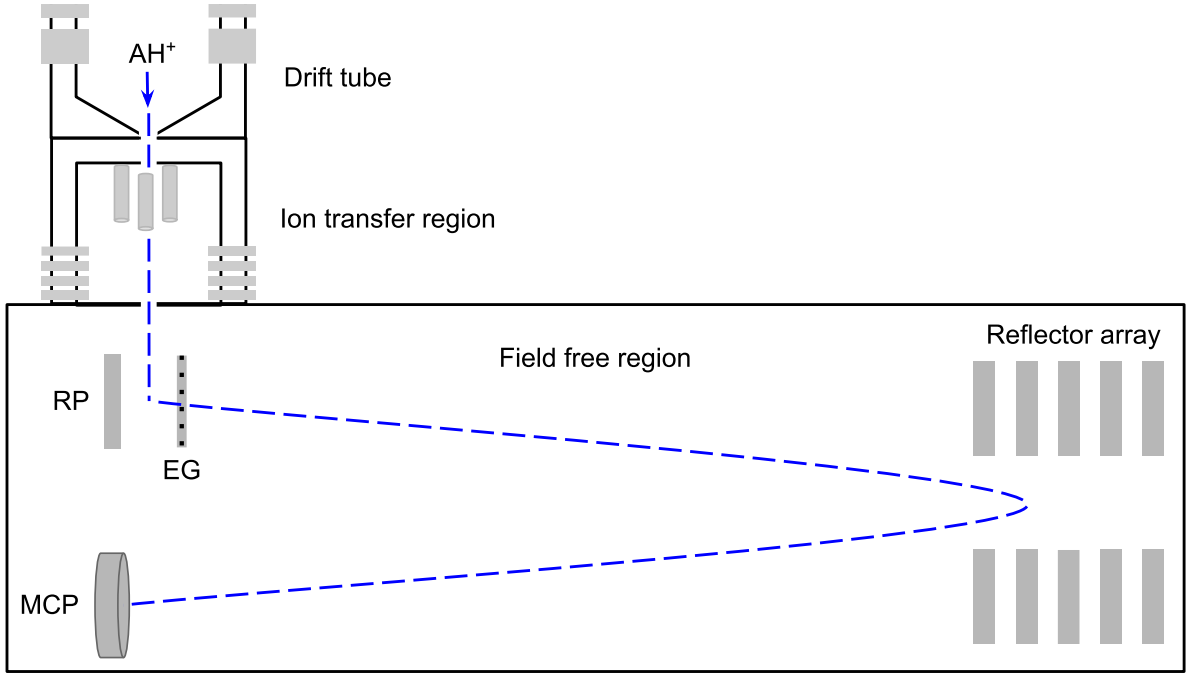


Figure 10. Schematic of an orthogonal acceleration Time-of-Flight mass analyzer (oa-ToF-MS), which includes a repeller plate (RE), an extractor grid (EG), a reflectron and a microchannel plate detector (MCP).

In general, a longer flight path improves the mass resolution, as it increases the spatial and temporal separation between ions with different *m/z*. Linear ToF-MS instruments have the simplest configuration, but reflectron ToF-MS is widely used for increasing the flight path and resolution without increasing the geometric footprint of the instrument. Reflectron ToF-MS includes a reflector array ("ion mirror") to reflect and direct the ions towards the detector, resulting in a V-shaped flight path. The reflector array is a series of electrodes with an increasingly repulsive potential. An additional benefit of reflectron TOF-MS is that the reflector array is an energy-focusing device, which corrects the ions energy spread and thereby increases the mass resolution.

As mentioned earlier, the pressure in the ToF is typically ~$10^{-6}$ mbar. The low pressure is necessary in order for the mean free path of the ions to be long enough to prevent collisions of ions with background gas.

The ions are detected using a microchannel plate (MCP) detector. MCP detectors are ~1 mm thick plates made of a highly resistive material filled with closely packed capillary tubes connecting the two ends. The capillaries are 3-20 µm in diameter and are lined with a semiconductor, e.g. lead oxide (PbO). There is a cathode at the entrance of the MCP and an anode at the exit of the MCP, and the potential difference across the plate is typically 2 kV.

When the ions enter the capillary tubes and collide with the walls of the tubes, they trigger an avalanche of secondary electrons. This amplifies the original signal by ~$10^3$ for a single MCP, but normally two or three MCPs are installed in a stack which amplifies the original signal by $10^6$-$10^8$. Since this amplified signal is still weak, the current is further amplified and currents above a threshold are converted into digital signals. The conversion process is done by a time-to-digital converter (TDC) and the signals are recorded and further processed by the data acquisition system.

For the analysis of the gas phase products emitted from the lake samples, a PTR-TOF 8000 instrument (Ionicon Analytik GmbH, Innsbruck, Austria) was used. The DT pressure was 2.2 mbar and the temperatures of the heated inlet and the DT were both set to 80°C. The E/N in the DT was 98 Td. The *m/z* range selected for this study was 0-386.

The PTR-MS Viewer (version 3.2.12; Ionicon Analytik GmbH, Innsbruck, Austria) was used for mass axis calibration, peak search, high-resolution peak fitting and peak integration. Further processing and statistical calculations were performed using Jupyter Notebook version 6.0.1 with a Python 3.7.4 kernel (Python Software Foundation, Delaware, United States).

All measurements were normalized to account for varying levels of primary ions in the PTR-MS instrument during measurements. This was done using the following equation (de Gouw et al. 2003):

$$N_i = \frac{s_i}{487 \times s_m + 244 \times s_d} \times 10^6 \quad (15)$$

Where $N_i$ is the signal of the selected *m/z* in ncps, $s_i$ is the signal of the selected *m/z* in cps, $s_m$ is the signal of $H_3O^+$ in cps and $s_d$ is the signal of $H_2O.H_3O^+$ in cps.

Calibration of the PTR-MS instrument was performed to determine instrument sensitivity. A VOC calibration gas standard (cylinder D540949, Apel-Riemer Environmental Inc., Miami, Florida, United States) containing 17 different VOCs was used for this purpose. The volume mixing ratio (VMR) of the calibration gas went through four steps and was continuously measured using the PTR-MS analyzer. The signal was normalized following the procedure described above, and a calibration curve was created for each compound in the calibration gas. The calibration curve is the average signal at each step plotted against the volume mixing ratio of the compound at that step. Figure 11 below shows the calibration curve of acetone as an example. The slope of the linear regression is the instrument sensitivity of the specific compound. The sensitivities for the compounds in the calibration can be found in

Table 2 below.

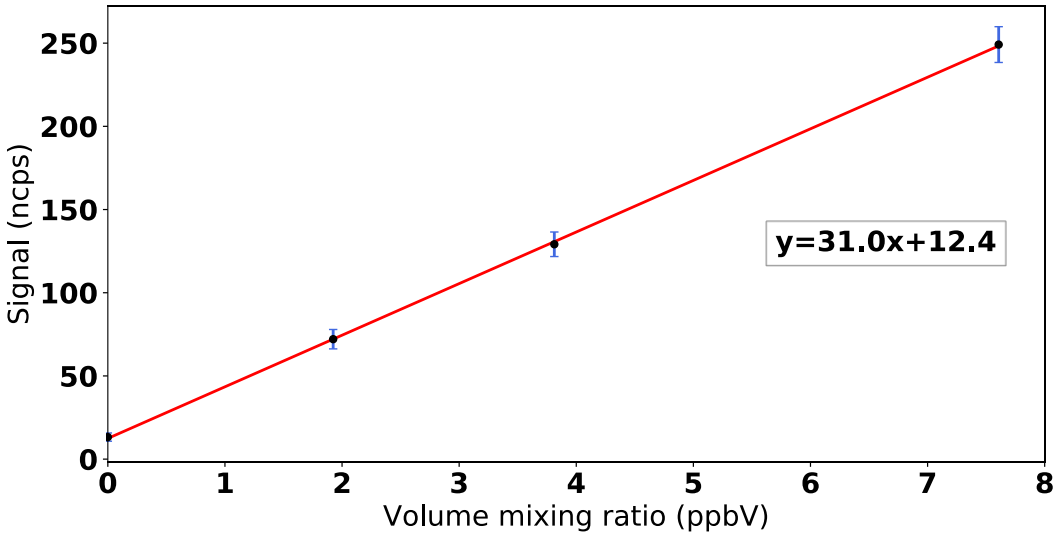


Figure 11. Calibration curve for acetone. The normalized mean signal in each calibration step is plotted against volume mixing ratio in ppbV. Linear regression line is shown in red and its function is y=31.0x+12.4.

Table 2. Sensitivities of the compounds in the calibration gas standard.

| Compound | *m/z* | Sensitivity (ncps/ppbV) | Limit of Detection (ppbV) |
|---|---|---|---|
| methanol | 33.03 | 11.6 | 1.27 |
| acetonitrile | 42.03 | 28.5 | 0.85 |
| acetaldehyde | 45.03 | 22.9 | 0.90 |
| acetone | 59.05 | 31.0 | 1.28 |
| methyl ethyl ketone | 73.07 | 34.6 | 0.38 |
| xylene | 107.09 | 25.6 | 0.12 |
| trimethylbenzene | 121.10 | 27.4 | 0.11 |
| triisopropylbenzene | 205.19 | 29.9 | 0.18 |

For methanol, acetaldehyde and acetone, the measured sensitivities were used to convert the signal (ncps) into VMRs (ppbV). Higher aldehydes were not individually calibrated. Instead, the acetone sensitivity was used for quantification, and higher aldehyde VMRs are thus reported as acetone-equivalents. This approach is reasonable because higher aldehydes typically react with $H_3O^+$ ions at a rate that is similar to that of acetone. In addition, at an E/N of 98 Td the fragmentation of protonated aldehydes is reduced. A more accurate quantification was

considered unnecessary, since I mostly investigated relative differences between different samples and exposure conditions.

A baseline subtraction was carried out for all the lake water samples. The average signal value measured during the ~2 minutes before exposure was subtracted from the signal measured during the exposure.

## 2.5 Ozone measurements

$O_3$ was measured using a 49C $O_3$ Analyzer (Thermo Environmental Instruments Inc., United States). The $O_3$ monitor is based on the principle that $O_3$ absorbs UV light at a wavelength of 254 nm. The amount of UV light absorbed is proportional to the $O_3$ concentration and is described by Beer-Lambert's law:

$$\frac{I}{I_0} = e^{-KLC} \tag{16}$$

where $I$ is the transmitted UV light through the sample with ozone, $I_0$ is the transmitted UV light through the reference, $K$ is the molecular absorption coefficient (308 $cm^{-1}$ at 0°C and 1 atm pressure), $L$ is the length of the cell (38 cm) and $C$ is the $O_3$ concentration in ppm.

The $O_3$ monitor contains a sample cell and a reference cell. The sample is drawn into the $O_3$ monitor before being split into two streams where one stream enters the sample cell and the other stream passes through an $O_3$ scrubber before entering the reference cell. The UV light that passes through each of the cells is measured and used to determine the $O_3$ concentration in the sample. The sample cell and reference cell are alternated every 10 seconds, and the light intensities are ignored for several seconds to allow the cells to be flushed before a new measurement. The switching of the cells is done to prevent artifacts, e.g. compounds being unequally retained in the two cells, which is of particular concern to the reference cell as ozone helps remove reactive compounds.

## 2.6 Total organic carbon analysis

The total organic carbon (TOC) analysis was performed by Berit Kaasa at the Department of Biosciences at the University of Oslo using a Shimadzu TOC-VCPH (Shimadzu, Kyoto, Japan).

The liquid sample was pumped into a combustion furnace which is supplied with purified air where it underwent combustion through heating to 680℃ with a platinum catalyst. It decomposed and was converted to $CO_2$ and NO. The gases were then cooled and dehumidified before entering the detector, where the ratio of total C to total N is obtained from the calibration curve.

The PTR-MS samples that were exposed for 3 hours to UV radiation, $O_3$, or both were analyzed for TOC before and after the exposures.

Five calibration solutions with potassium hydrogen phthalate (CAS 877-24-7, Merck KGaA, Darmstadt, Germany) were prepared for total organic carbon (TOC) analysis. First potassium hydrogen phthalate was heated in an oven at 115℃ for at least one hour to remove water. Then 0.2125 g was weighed out, transferred to a 1000 mL volumetric flask, and diluted to the mark. Five different concentrations were prepared from this 100 mg TOC $L^{-1}$ stock solution. The final concentrations of the calibration solutions were 0, 1, 5, 15 and 50 mg $L^{-1}$. Samples and calibration solutions were kept in 50 mL plastic containers and frozen until analysis.

# 3 Results and Discussion

The focus of this investigation was to study the effect of UV radiation and atmospheric ozone on the emission of VOCs from lake water. This was to gain a deeper understanding of the processes involved in the loss of carbon from lakes into the atmosphere and the role of bulk water and the SML as sources of VOCs in lakes with different properties.

In the following text, the term "photooxidation" only refers to UV-induced processed and does not include ozonolysis.

## 3.1 Total organic carbon content

The TOC content was primarily measured to aid the interpretation of the PTR-MS results. TOC levels in the bulk water samples were in the range between 1.912 and 20.25 mg $L^{-1}$. Table 3 lists the TOC content in the bulk water samples and some SML samples. The latter consisted of 25% (v/v) SML mixed with bulk water from the same lake. For 5 samples, the TOC content was measured before and after a 3 hour exposure to UV light and/or ozone to see if the volatilization of carbon results in a measurable change of the TOC content.

Table 3. Total organic carbon content in the lake water samples. The SML samples consisted of 25% SML and 75% bulk water. N/A: not analyzed

| Lake/ sample | Before exposure (mg/L) | After 3h exposure (mg/L) | | |
|---|---|---|---|---|
| | | UV | UV+$O_3$ | $O_3$ |
| Lutvann | 1.912 | N/A | N/A | N/A |
| Kolbotn | 4.390 | N/A | N/A | N/A |
| Østensjøvann | 5.965 | N/A | N/A | N/A |
| Gjersjøen | 6.272 | N/A | N/A | N/A |
| Årungen | 6.594 | N/A | N/A | N/A |
| Svartkulp | 7.966 | N/A | N/A | N/A |
| Sværsvann | 10.46 | N/A | N/A | N/A |
| Tjernsrudtjern SML | 11.56 | 13.22 | 14.01 | 13.18 |
| Tjernsrudtjern | 12.44 | 12.45 | 12.72 | 12.54 |
| Tennungen | 13.32 | 12.66 | 12.91 | 13.55 |
| Tennungen SML | 17.34 | 16.51 | 16.51 | 17.84 |
| Sessvoldtjern | 20.25 | 18.81 | 18.84 | 20.14 |

The increase in TOC levels in the two Tjernsrudtjern samples after exposure may be explained by the presence of plant debris decomposing upon exposure to UV and or ozone. Only the Tjernsrudtjern samples contained a substantial amount of plant debris. In the Sessvoldtjern, Tennungen and Tennungen SML samples there is some indication that exposure to UV light decreased the TOC levels. The measured decrease is about 3-7%.

## 3.2 Proton-transfer-reaction mass spectrometer results

The PTR-MS results are presented in twelve subchapters, one for each compound studied. The whole m/z range was manually scanned for signals increasing upon exposure. Twelve signals exhibited a consistent and significant increase and were thus studied in greater detail. The 12 m/z signals were assigned to the following compounds: m/z 33.03: methanol, m/z 45.03: acetaldehyde, m/z 59.05: acetone/propanal, m/z 87.08: pentanal, m/z 101.09: hexanal, m/z 115.11: heptanal, m/z 129.13: octanal, m/z 143.14: nonanal, m/z 157.16: decanal, m/z 171.17: undecanal, m/z 211.24: pentadecene, and m/z 239.27: heptadecene. It was not possible to measure m/z 73.06 (butanal) because of the interference from the (H2O)3.H3O+ ion at m/z 73.048. It is worth noting that, while similar studies found high emissions of unsaturated aldehydes from SML samples exposed to UV light (Fu et al. 2015; Ciuraru et al. 2015b), this was not observed in this study.

Four different experiments were executed: i) short-term (minutes to tens of minutes) exposure of samples from all ten lakes, ii) 3 h exposure of samples from three lakes, iii) variation of UV intensity upon exposure of a sample from one on emission level, iv) effect of filtration on emissions from one lake.

In experiment i) all lake bulk water samples were exposed for 4-20 minutes while the headspace was analyzed. The exposure time was not the same for all samples; the measurement was stopped when acetaldehyde and nonanal levels had stabilized. This resulted in varying exposure times. An HPLC water blank measurement was included as a reference, and I will be showing the mean signal of all the blank measurements taken before each of the samples. This includes 10 blanks for each exposure, one for each lake sample. The standard deviations are the shaded areas. Since the length of the blank measurements also differed, the standard deviation was only calculated for the time period where there was data from at least 3 samples. This occurred only in the first ~12 minutes after exposure. It was possible to calculate the mean for less than three blank measurements, which is why the mean trace is longer than the standard deviation.

In experiment ii), samples from three of the lakes were exposed for three hours to observe emissions on a longer time scale than in experiment i). I studied both bulk water samples and SML samples to study potential differences in VOC emissions. The Tjernsrudtjern and Tennungen SML samples consisted of 50 mL of SML sample mixed with 150 mL bulk water from the same lake. The Sessvoldtjern SML sample was a 100% SML sample. The HPLC water blank was done separately from the samples, and only one three hour HPLC water measurement that was done. The PTFE tubes and sample vessel were flushed for longer before the blank measurement was done than before the lake samples were measured. The equipment was therefore most likely cleaner before the blank measurement than when the samples were measured, which could lead to an overestimation of the emissions from the samples. Comparing the levels and trends in emissions from the lakes relative to each other is more useful and meaningful in this case.

Experiment iii) was carried out to study the effect of UV intensity on VOC emissions. Samples from Tjernsrudtjern bulk water were exposed to four different UV intensities. The intensities were set to 0.10, 0.20, 0.35 and 0.68 W m-2 measured at 340 nm by a sensor inside the Q-SUN instrument.

Experiment iv) was carried out to examine the potential contribution from microbiological sources to VOC emissions. As described in section 2.2, water from the Svartkulp lake was either left unfiltered or filtered (0.2 µm, 0.45 µm). The three samples were exposed to the same conditions and compared.

### 3.2.1 Methanol

Figure 12 presents the emissions of methanol (*m/z* 33.03) from each of the lake samples upon exposure to UV, UV and $O_3$ and $O_3$ only, respectively.

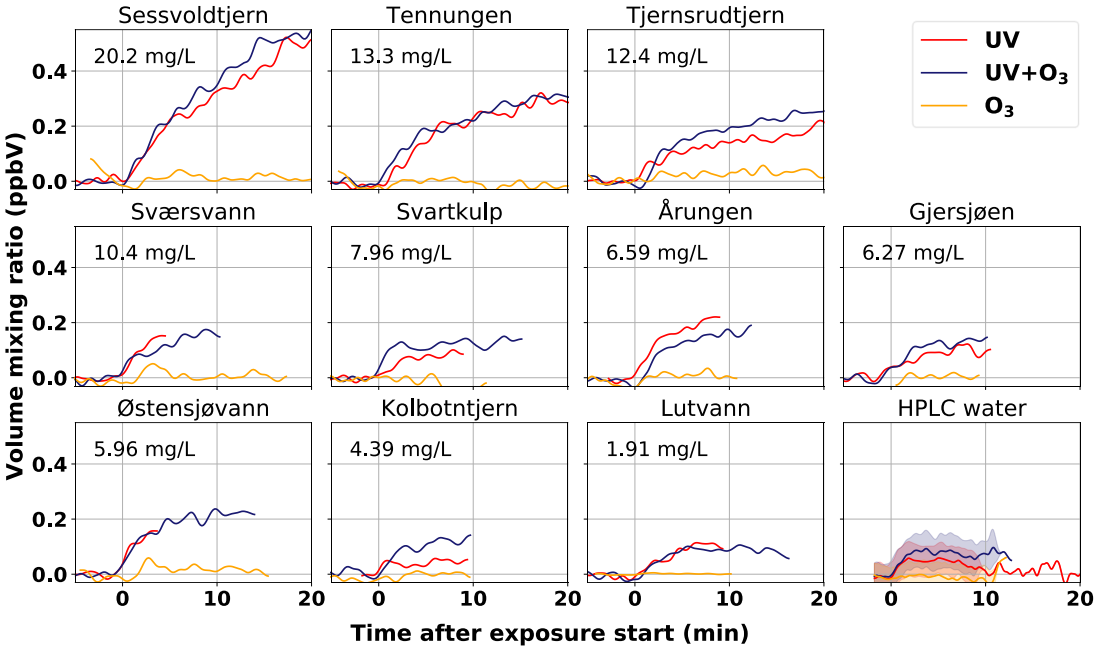


Figure 12. Volume mixing ratios of methanol observed in the dynamic headspace of water samples obtained from ten Norwegian lakes upon exposure to UV, UV and $O_3$ and $O_3$, respectively. The TOC content of the sample is given in the upper left corner of the subplot. The "HPLC water" subplot shows the mean signal (plus standard deviation in shading) from the HPLC water blank measurements carried out before each measurement.

Methanol was only emitted with UV light present, i.e. in the UV and UV+$O_3$ conditions. The UV intensity was the same for both conditions yielding similar amounts of methanol, with $O_3$ having no effect. There were some emissions from the HPLC water blank samples, but levels were low. Methanol emissions from the Sessvoldtjern and Tennungen samples peaked at 0.5 and 0.3 ppbV, respectively, and these lakes had the highest TOC content. The samples from Østensjøvann, Årungen, Tjernsrudtjern and Sværsvann exhibited similar increases in methanol emissions during the UV and UV+$O_3$ exposures. For most samples methanol increased during the first few minutes and then flattened out. In case of the Sessvoldtjern, Tennungen and Tjernsrudtjern samples, which had the highest TOC content, the increase continued past the first 20 minutes of exposure. These samples were additionally subjected to a 3-hour exposure (Figure 13), but even then no flattening out was observed. The emission of methanol were proportional to the TOC levels in these samples. The Sessvoldtjern sample had the highest TOC level at 20.2 mg $L^{-1}$, and maximum methanol volume mixing ratios exceeding 1.7 ppbV were observed. In the Tennungen sample with a TOC content of 13.3 mg $L^{-1}$ the maximum methanol volume mixing ratio was 1.5 ppbV, and in the Tjernsrudtjern sample with a TOC content of 12.4 mg $L^{-1}$ the maximum methanol volume mixing ratio was about 0.9 ppbV. The SML and

bulk water samples from the Sessvoldtjern lake showed no differences in methanol emissions, while in the Tjernsrudtjern sample more methanol was produced from the SML. In the Tennungen samples, methanol emissions were lower from the SML.

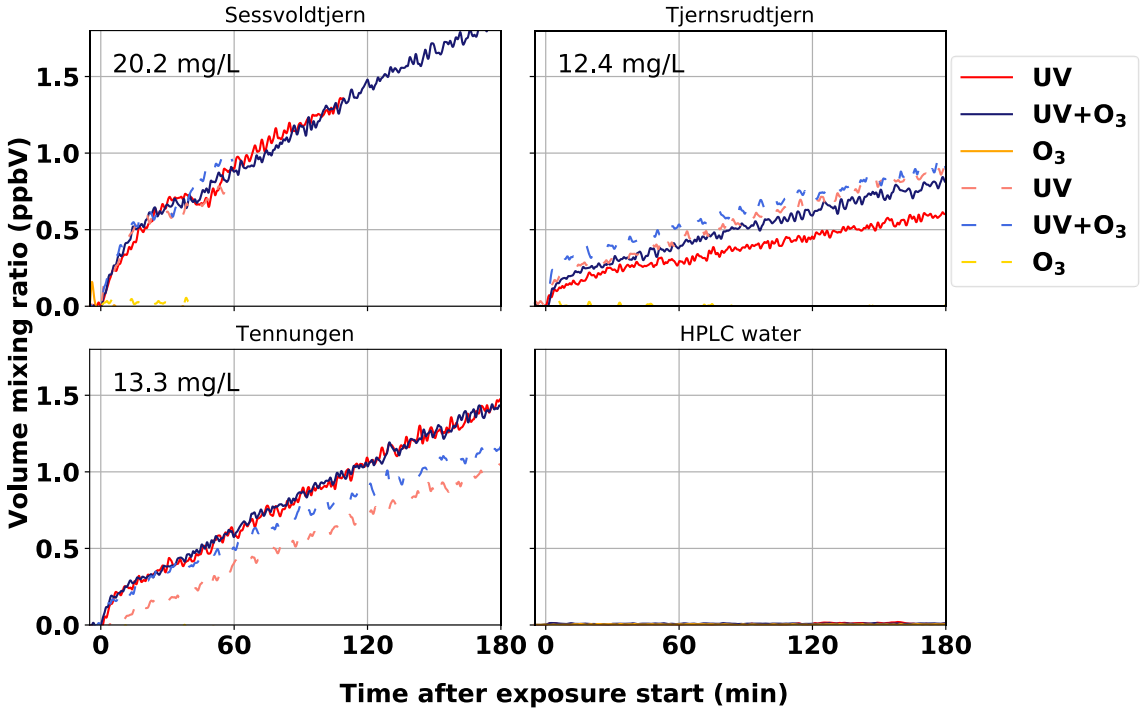


Figure 13. Volume mixing ratios of methanol observed in the dynamic headspace of water samples (SML: dashed lines, bulk: solid lines) obtained from the Sessvoldtjern, Tjernsrudtjern, and Tennungen lakes upon 3-hour exposure to UV, UV and $O_3$, and $O_3$, respectively.

The results shown in Figure 14 suggest that methanol emissions increased with UV light intensity. A pronounced effect was only seen at the highest UV intensity, 0.68 W $m^{-2}$. There was no observable difference in methanol emissions from the 0.2 µm filtered, 0.45 µm filtered and unfiltered samples taken from the Svartkulp lake (Figure 15).

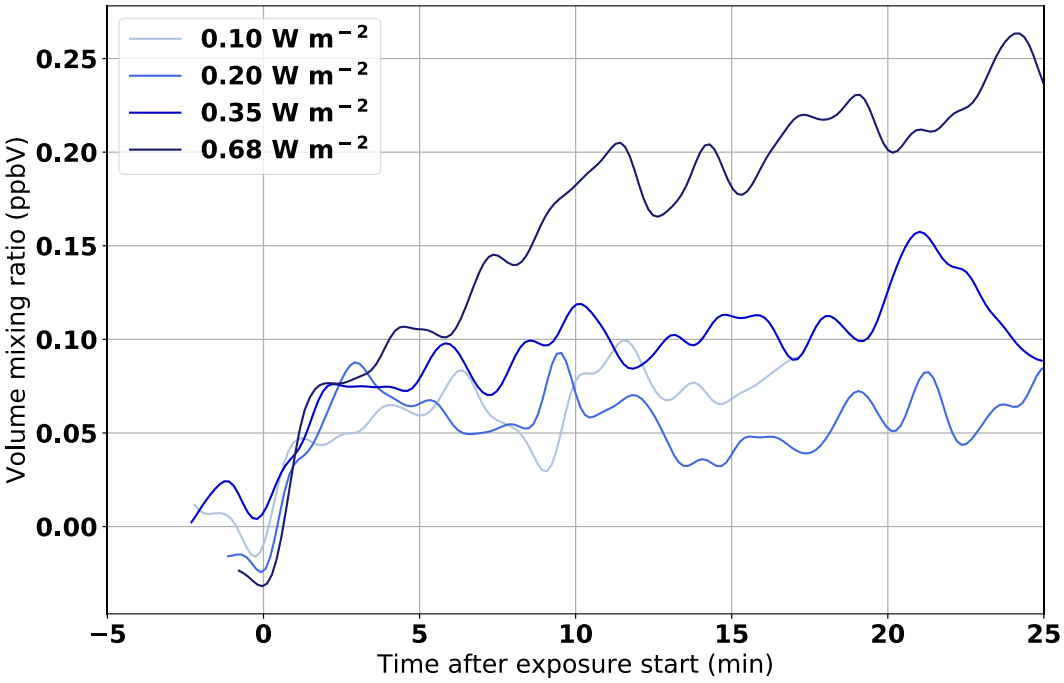


Figure 14. Volume mixing ratios of methanol observed in the dynamic headspace of water samples obtained from the Tjernsrudtjern lake upon exposure to different UV light intensities.

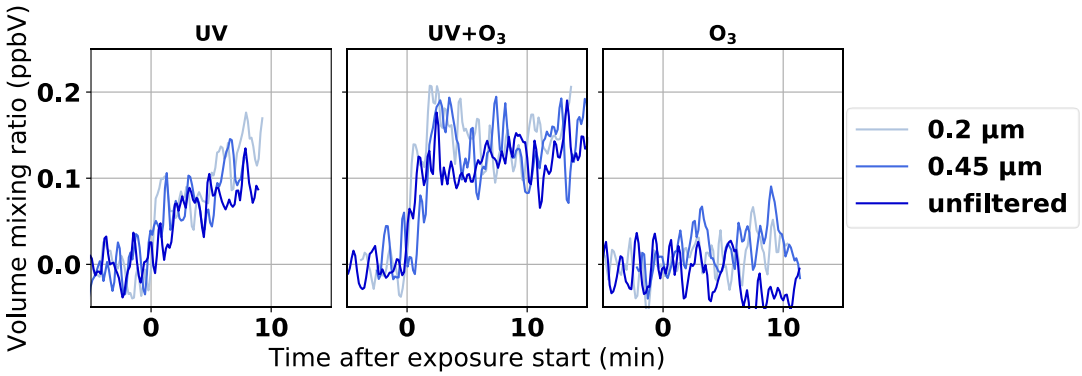


Figure 15. Volume mixing ratios of methanol observed in the dynamic headspace of filtered (0.2 µm and 0.45 µm) water samples and an unfiltered water sample from the Svartkulp lake upon exposure to UV, UV and $O_3$, and $O_3$, respectively.

The results presented in Figures 12-15 indicate that methanol is produced through UV-light induced processes, while exposure to $O_3$ does not form methanol. There are large differences in methanol emissions from different lake water samples, but higher methanol emissions were found for samples with higher TOC content. Methanol emissions from the Sessvoldtjern, Tennungen and Tjernsrudtjern samples continued to increase over three hours of UV exposure, indicating that the precursor material is not depleted rapidly and thus present in significant amounts. Filtration of the water samples did not affect methanol emissions, suggesting that methanol derives from dissolved carbon. Since methanol is only produced through UV-induced

processes and is formed in the sterilized sample, this is a strong indication that methanol observed is formed through photooxidation and not by biological activity. No clear trend of increased emissions of methanol from the SML was observed.

### 3.2.2 Acetaldehyde

Figure 16 shows the emissions of acetaldehyde (m/z 45.03) from each of the lake samples upon exposure to UV, UV and $O_3$ and $O_3$ only, respectively. Acetaldehyde was only produced in the presence of UV light, i.e. in UV and UV+$O_3$ conditions, and the emissions were similar for most of the samples. For the Østensjøvann, Årungen and Sværsvann samples less acetaldehyde was formed in the UV+$O_3$ condition, which is probably just a result of the natural variability between samples from the same batch. No significant acetaldehyde emissions were observed when the samples were exposed to $O_3$ only.

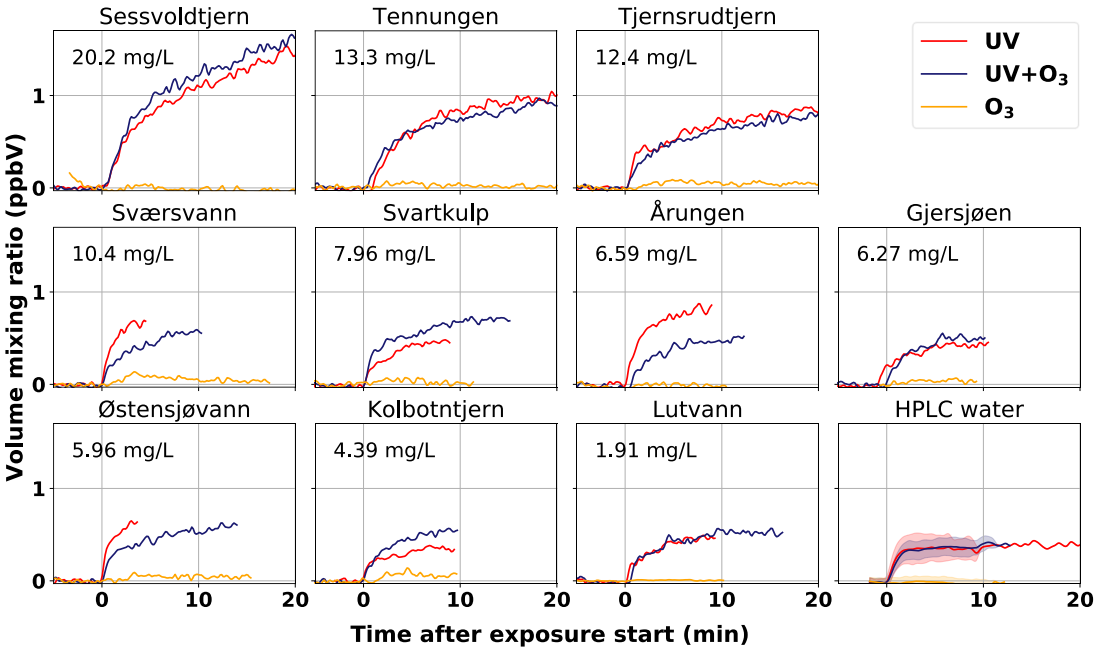


Figure 16. Volume mixing ratios of acetaldehyde observed in the dynamic headspace of water samples obtained from ten Norwegian lakes upon exposure to UV, UV and $O_3$ and $O_3$, respectively. The TOC content of the sample is given in the upper left corner of the subplot. The "HPLC water" subplot shows the mean signal (plus standard deviation in shading) from the HPLC water blank measurements carried out before each measurement.

Similar to methanol, for most of the samples the volume mixing ratio of acetaldehyde rapidly increased during the first few minutes of exposure before flattening out. The lake water samples with the highest TOC levels produced the highest emissions of acetaldehyde, while samples

with low TOC formed little acetaldehyde. In the case of the Lutvann sample, which had the lowest TOC content of all lakes, emissions of acetaldehyde were similar to those observed for the HPLC water blank sample. This could indicate that the emissions observed from the Lutvann sample are just experimental artifacts and not emissions from the sample itself.

During the 3-hour exposure to UV and UV+$O_3$, acetaldehyde exhibited a steep initial rise which was followed by a linear increase (Figure 17). In the dynamic headspace of the Sessvoldtjern lake the highest acetaldehyde volume mixing ratios of ~ 4 ppbV were observed, while in the Tennungen and Tjernsrudtjern samples acetaldehyde reached maxima of 2.7 ppbV and 2.3 ppbV respectively. There was no difference in SML and bulk water emissions in the Sessvoldtjern samples, while in the Tennungen samples more acetaldehyde was formed from the SML. The opposite was observed for the Tennungen samples.

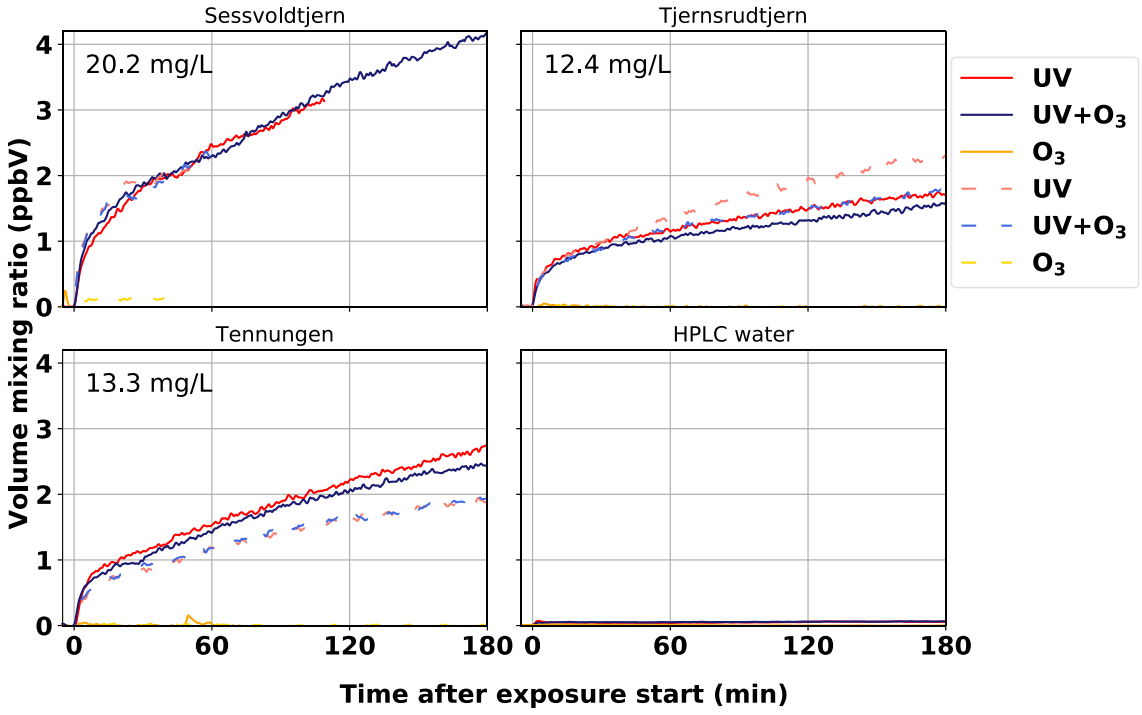


Figure 17. Volume mixing ratios of acetaldehyde observed in the dynamic headspace of water samples (SML: dashed lines, bulk: solid lines) obtained from the Sessvoldtjern, Tjernsrudtjern, and Tennungen lakes upon 3-hour exposure to UV, UV and $O_3$, and $O_3$, respectively.

The results shown in Figure 17 show that acetaldehyde emissions increased with UV light intensity. This effect was very pronounced at the highest UV light intensity of 0.68 W $m^{-2}$.

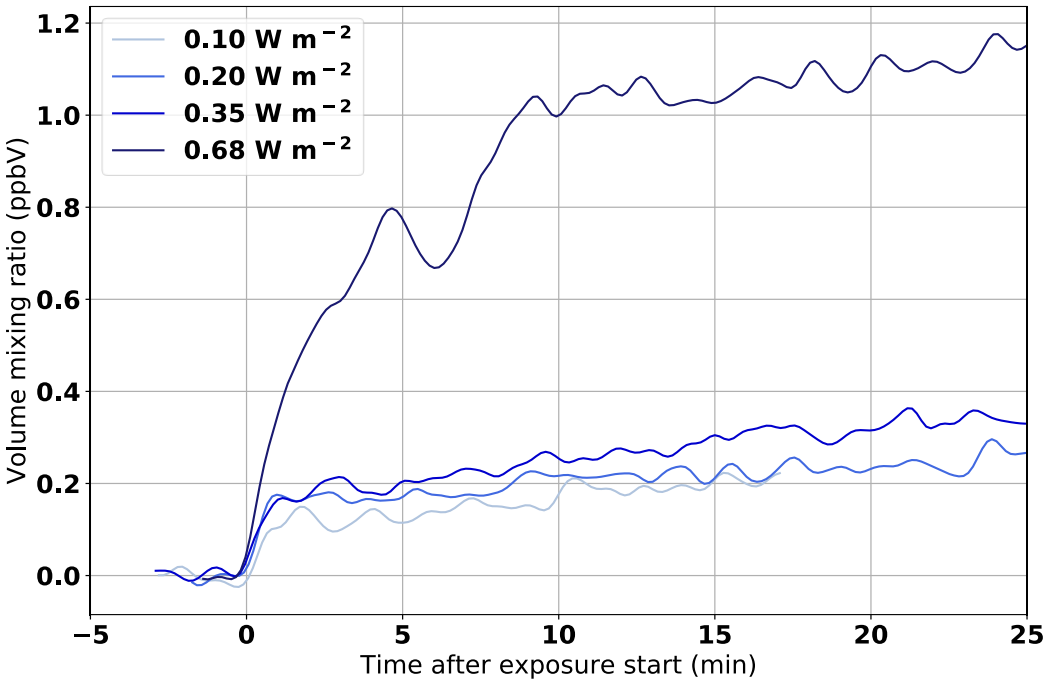


Figure 18. Volume mixing ratios of acetaldehyde observed in the dynamic headspace of water samples obtained from the Tjernsrudtjern lake upon exposure to different UV light intensities.

Upon UV exposure, the filtered and unfiltered samples from Svartkulp emitted similar amounts of acetaldehyde (see Figure 19). Upon the UV+$O_3$ exposure, the 0.45 µm filtered sample emitted higher levels of acetaldehyde than the other two samples. This was probably again caused by the natural variability between samples from the same batch. Figure 19 shows negative volume mixing ratios for the $O_3$ only condition. This was most likely caused by an elevated background level measured before the start of that experiment.

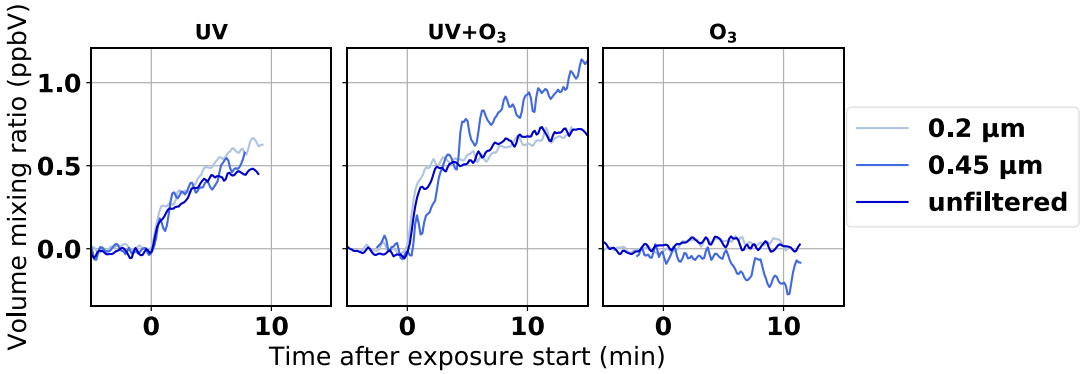


Figure 19. Volume mixing ratios of acetaldehyde observed in the dynamic headspace of filtered (0.2 µm and 0.45 µm) water samples and an unfiltered water sample from the Svartkulp lake upon exposure to UV, UV and $O_3$, and $O_3$, respectively.

The observations made for acetaldehyde closely resemble what was found for methanol. Acetaldehyde appears to be formed through a UV-induced process and not via ozonolysis. The

precursor substance(s) are abundant and are not depleted in the time frame of hours. Filtration of the water samples did not affect acetaldehyde emissions, suggesting that dissolved organic carbon acts as a precursor for the acetaldehyde being emitted.

### 3.2.3 Acetone/propanal

Since acetone and propanal are isomers, it is impossible to separate them based on their m/z. Therefore, they are referred to here as acetone/propanal. Figure 20 shows the emissions of acetone/propanal (m/z 59.05) from each of the lake samples upon exposure to UV, UV+$O_3$ and $O_3$ only, respectively.

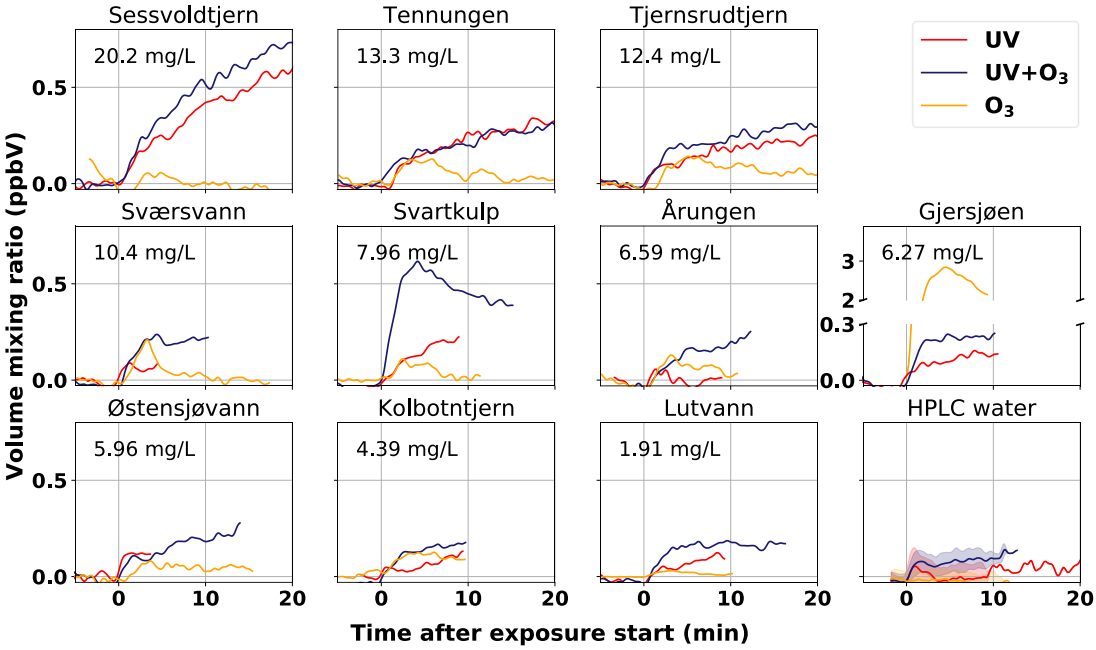


Figure 20. Volume mixing ratios of acetone/propanal observed in the dynamic headspace of water samples obtained from ten Norwegian lakes upon exposure to UV, UV and $O_3$ and $O_3$, respectively. The TOC content of the sample is given in the upper left corner of the subplot. The "HPLC water" subplot shows the mean signal (plus standard deviation in shading) from the HPLC water blank measurements carried out before each measurement. Note that the y-axis for the Gjersjøen lake subplot differs from the rest.

Contrary to methanol and acetaldehyde, acetone/propanal was also emitted when lake water samples were exposed to ozone only. Emissions were temporary, i.e. they rose quickly, reached a maximum and decayed within a few minutes. This was true for most samples indicating that they contained a precursor reservoir, which reacted and got rapidly depleted. The Gjersjøen lake samples emitted the highest amount of acetone/propanal, which reached a maximum volume mixing ratio of 2.9 ppbV. Acetone/propanal was, however, also emitted in the UV only

condition. The Sessvoldtjern lake sample emitted relatively high concentrations of acetone/propanal upon exposure to UV light, both with and without ozone being present. In the 3-hour exposure experiments, acetone/propanal increased steeply at the beginning and the continued to grow linearly. The Sessvoldtjern and Tjernsrudtjern samples exhibited little to no differences in acetone/propanal emissions from the SML and the bulk samples. The SML sample from the Tennungen lake showed somewhat lower emissions than the bulk samples.

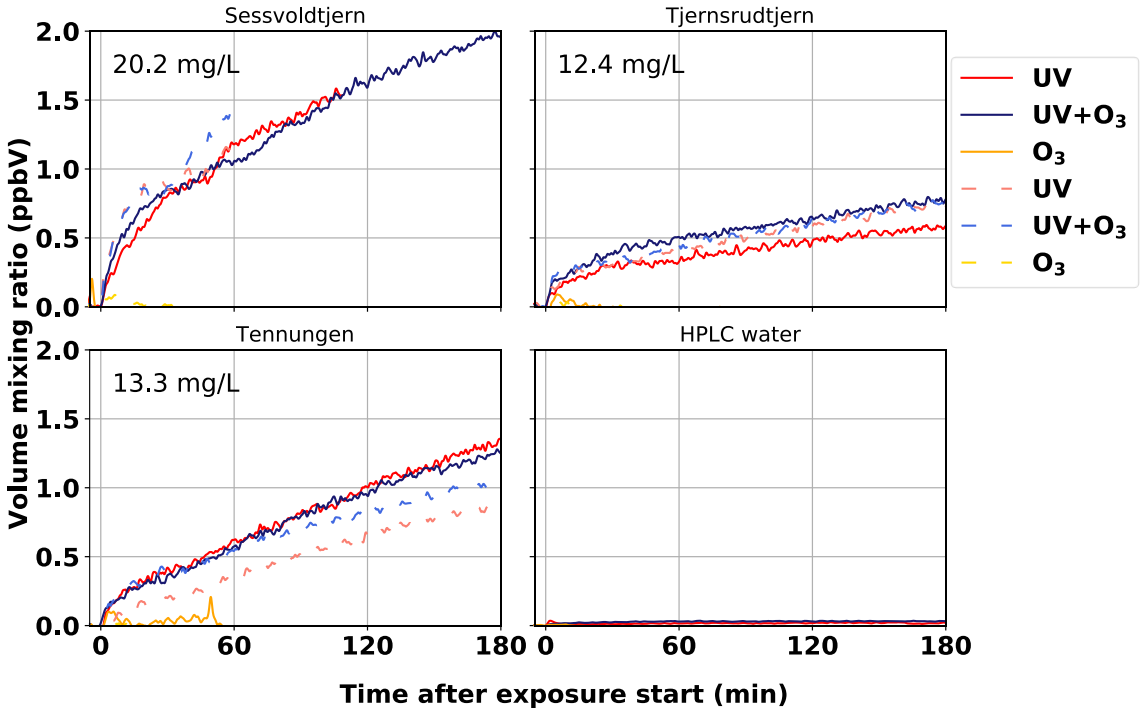


Figure 21. Volume mixing ratios of acetone/propanal observed in the dynamic headspace of water samples (SML: dashed lines, bulk: solid lines) obtained from the Sessvoldtjern, Tjernsrudtjern, and Tennungen lakes upon 3-hour exposure to UV, UV and $O_3$, and $O_3$, respectively.

Exposure to UV light intensities of 0.10, 0.20 and 0.35 W $m^{-2}$ resulted in similar acetone/propanal emission levels. A pronounced increase of acetone/propanal emissions was only observed at the highest UV light intensity of 0.68 W $m^{-2}$.

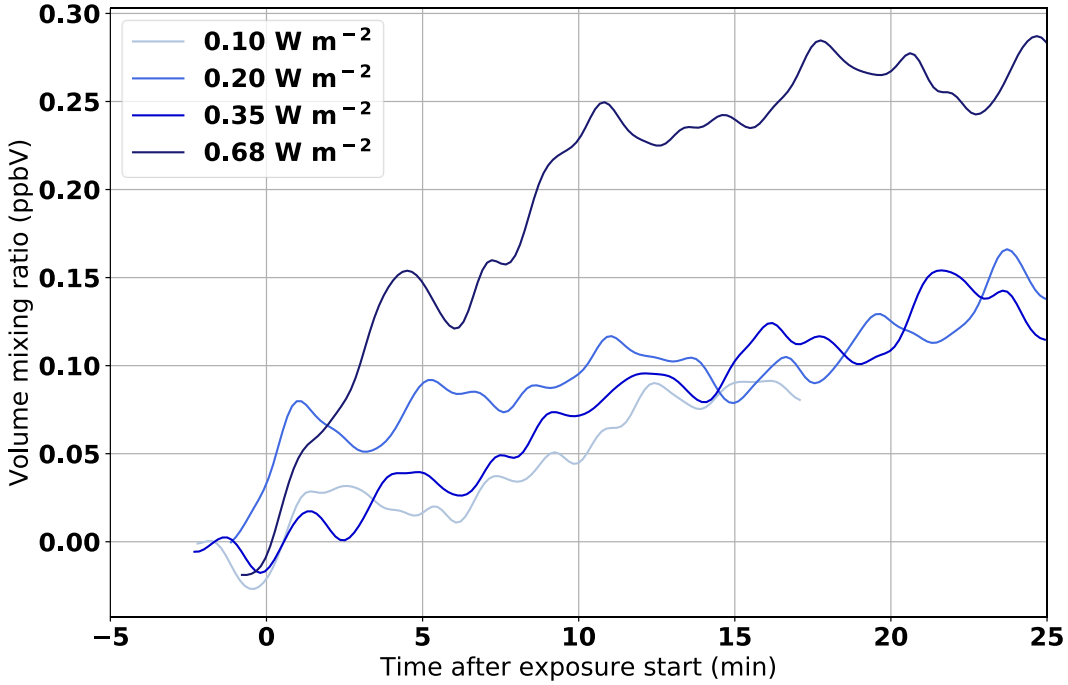


Figure 22. Volume mixing ratios of acetone/propanal observed in the dynamic headspace of water samples obtained from the Tjernsrudtjern lake upon exposure to different UV light intensities.

No differences in acetone/propanal emissions were observed when the sample from the Svartkulp lake was exposed to only $O_3$ or only UV light (Figure 23). Upon exposure to both UV and $O_3$ exposure, the 0.2 µm filtered and unfiltered samples emitted about the same level of acetone/propanal, while the 0.45 µm filtered sample exhibited lower emissions. This may, however, again be explained by the natural variability between samples of the same batch.

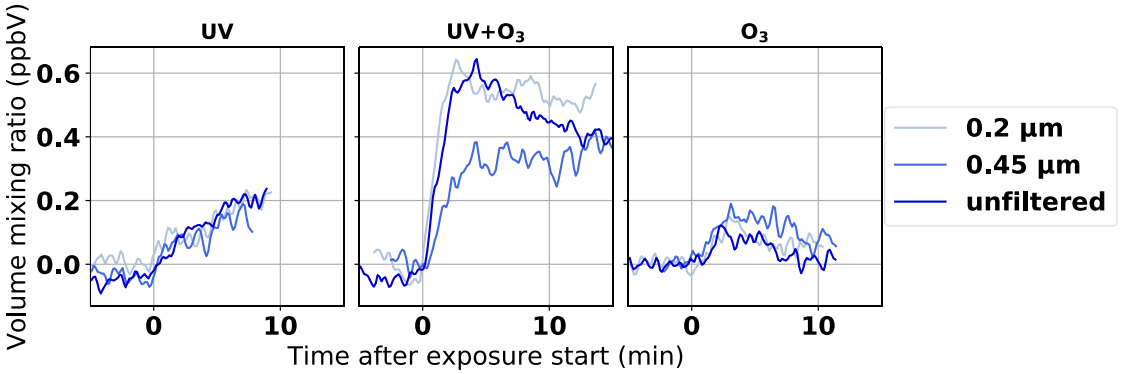


Figure 23. Volume mixing ratios of acetone/propanal observed in the dynamic headspace of filtered (0.2 µm and 0.45 µm) water samples and an unfiltered water sample from the Svartkulp lake upon exposure to UV, UV and $O_3$, and $O_3$, respectively.

Based on the presented results it is difficult to see and explain systematic differences between the different exposure conditions and samples. There is a general correlation between the TOC

concentrations and the emissions of acetone/propanal, but there are likely other unknown factors playing an important role in determining the emission levels. Acetone/propanal appears to be formed via different mechanisms, with either UV light or ozone being the driver. The latter may react with Zhou and co-workers (2014). Since acetone and propanal may be produced from different precursors and through different reaction mechanisms, and we only observed the sum of their emissions, it is difficult to separate them and assign their formation mechanism.

### 3.2.4 Pentanal

Figure 24 shows the emissions of pentanal (m/z 59.05) from each of the lake samples upon exposure to UV, UV+$O_3$ and $O_3$ only, respectively.

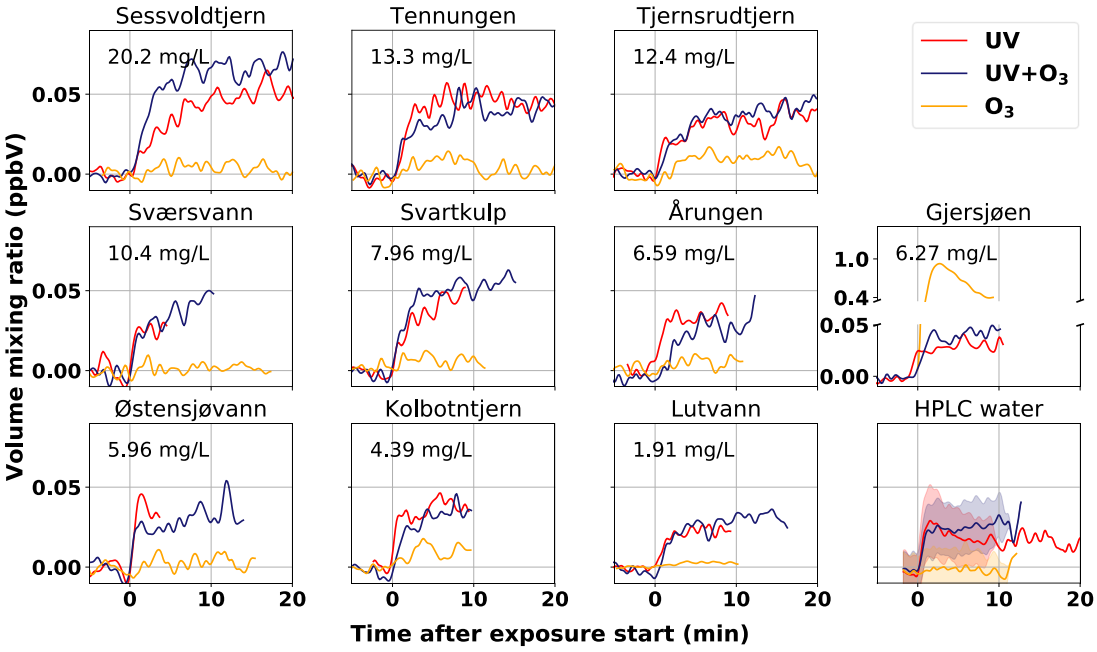


Figure 24. Volume mixing ratios of pentanal observed in the dynamic headspace of water samples obtained from ten Norwegian lakes upon exposure to UV, UV and $O_3$ and $O_3$, respectively. The TOC content of the sample is given in the upper left corner of the subplot. The "HPLC water" subplot shows the mean signal (plus standard deviation in shading) from the HPLC water blank measurements carried out before each measurement. Note that the y-axis for the Gjersjøen lake subplot differs from the rest.

The emission of pentanal from the lakes was observed to be low and most emissions from the samples were similar to the blank measurement (see Figure 24). The emissions from Gjersjøen

during the $O_3$ exposure were very high and increase up to nearly 1 ppbV. The other lakes showed negligible emissions from the $O_3$ exposure only.

The SML was not observed to enhance the emissions of pentanal from our samples (see Figure 25). The emission of pentanal during the UV and UV+$O_3$ exposure in Sessvoldtjern, Tennungen and Tjernsrudtjern increased in the first few minutes before stabilizing. The emissions from Sessvoldtjern and Tennungen continue to slowly increase over the 3 h exposure, while the emissions from Tjernsrudtjern flatten out.

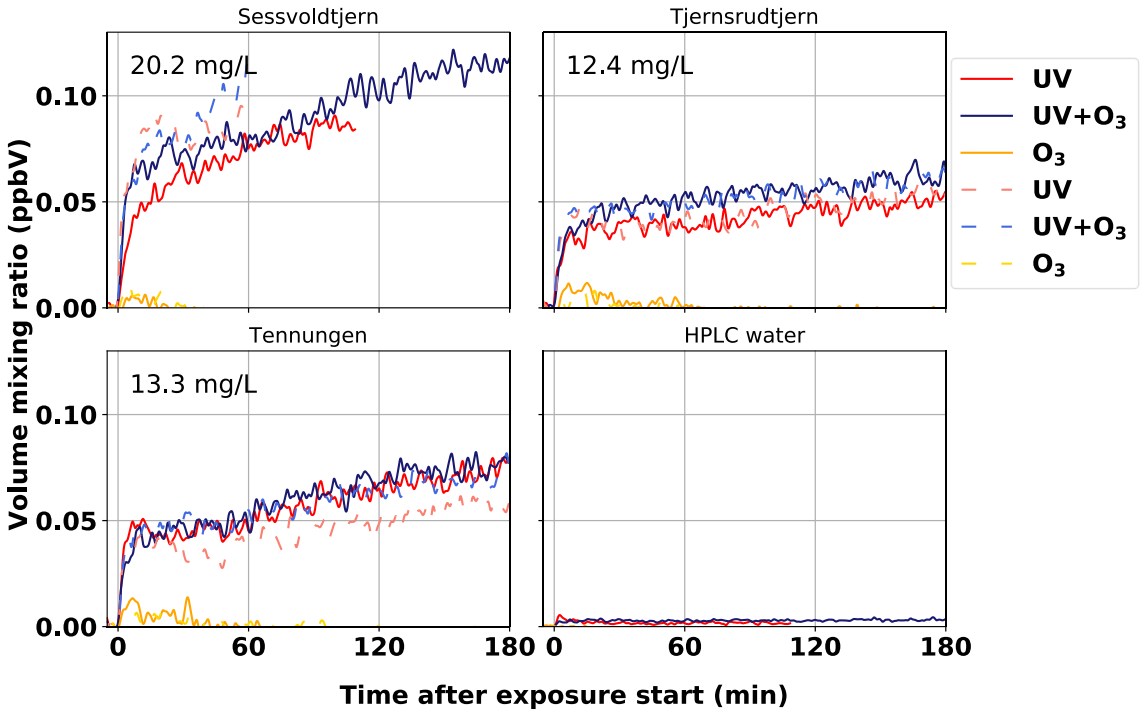


Figure 25. Volume mixing ratios of pentanal observed in the dynamic headspace of water samples (SML: dashed lines, bulk: solid lines) obtained from the Sessvoldtjern, Tjernsrudtjern, and Tennungen lakes upon 3-hour exposure to UV, UV and $O_3$, and $O_3$, respectively.

The 0.68 W $m^{-2}$ exposure caused the highest emission of pentanal, and the other three UV intensities induced lower pentanal emissions with similar levels (see Figure 26).

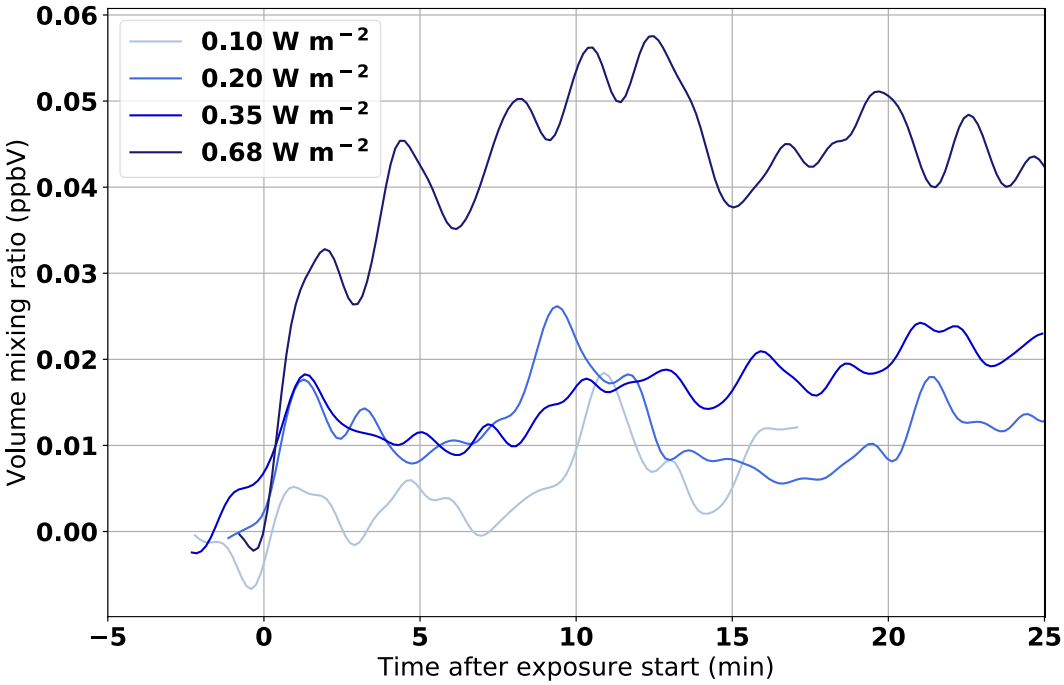


Figure 26. Volume mixing ratios of pentanal observed in the dynamic headspace of water samples obtained from the Tjernsrudtjern lake upon exposure to different UV light intensities.

No significant differences in the emission of pentanal from 0.2 µm filtered, 0.45 µm filtered and unfiltered samples from Svartkulp lake were observed (see Figure 27).

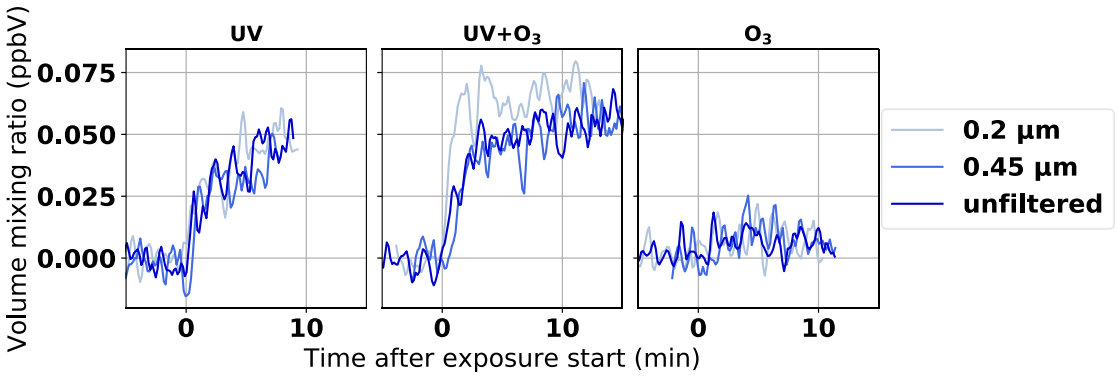


Figure 27. Volume mixing ratios of pentanal observed in the dynamic headspace of filtered (0.2 µm and 0.45 µm) water samples and an unfiltered water sample from the Svartkulp lake upon exposure to UV, UV and $O_3$, and $O_3$, respectively.

The emissions of pentanal from most lake samples were very low, at around 50 pptV. This was in the same order of magnitude as the blank measurement, indicating that what we observed was the background. Gjersjøen lake sample exposed to $O_3$ emitted high volume mixing ratios of pentanal, which could be formed through the ozonolysis of unsaturated fatty acids as proposed by Zhou and co-workers (2014). The SML did not produce higher emissions of

pentanal than the bulk water samples. High UV intensities did produce higher emissions of pentanal than lower UV intensities, indicating a correlation between UV intensity and emissions. Filtration of the lake water samples did not affect pentanal emissions, indicating that pentanal is formed from dissolved organic compounds.

### 3.2.5 Hexanal

Figure 28 shows the emissions of hexanal (m/z 101.09) from each of the lake samples during exposure to UV, UV+$O_3$ and $O_3$ only, respectively.

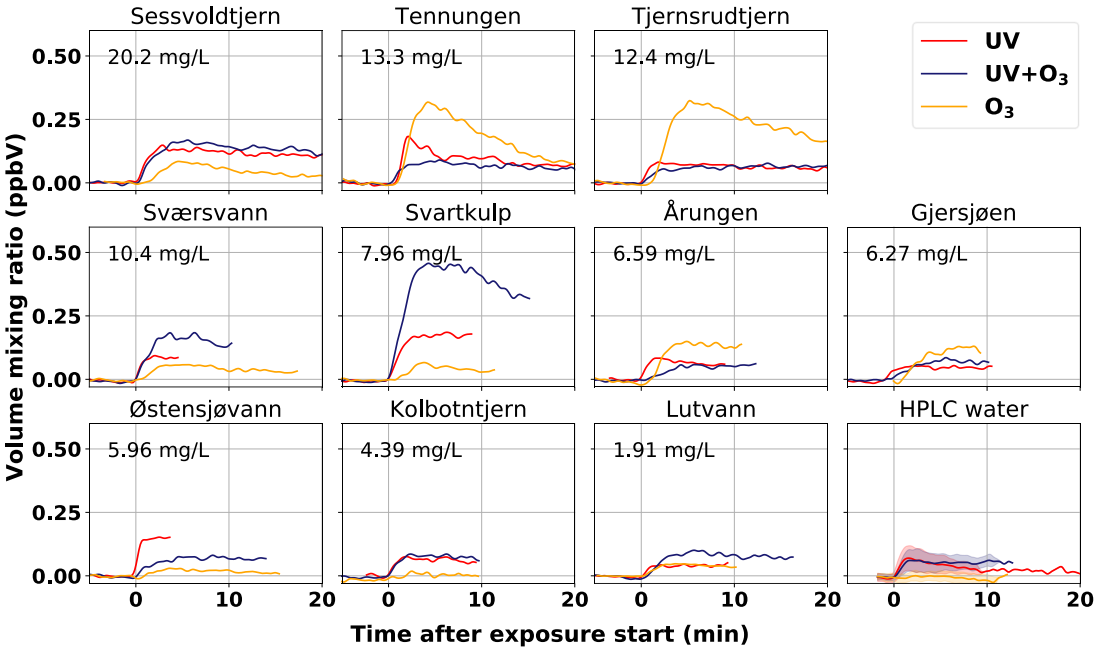


Figure 28. Volume mixing ratios of hexanal observed in the dynamic headspace of water samples obtained from ten Norwegian lakes upon exposure to UV, UV and $O_3$ and $O_3$, respectively. The TOC content of the sample is given in the upper left corner of the subplot. The "HPLC water" subplot shows the mean signal (plus standard deviation in shading) from the HPLC water blank measurements carried out before each measurement.

During exposure to $O_3$, high volume mixing ratios of hexanal were emitted from Årungen, Tennungen and Tjernsrudtjern lake samples. Svartkulp, Lutvann, Østensjøvann, Gjersjøen, Sværsvann and Sessvoldtjern were observed to emit small volume mixing ratios of hexanal during exposure to $O_3$. From the Svartkulp sample, the emissions were high during exposure to UV+$O_3$. Emissions displayed varying trends; all of them rose quickly, but some flattened out

at the maximum and others slowly decreased (see Figure 29). Generally, the emissions from the SML samples are quite similar to the bulk water samples.

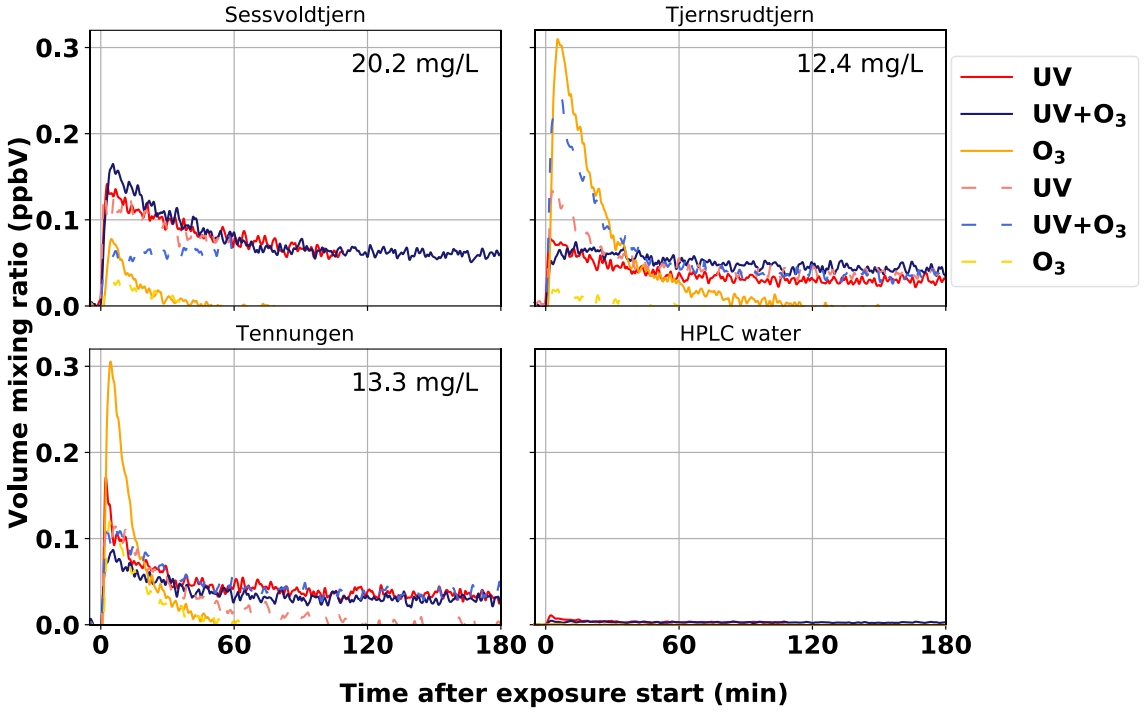


Figure 29. Volume mixing ratios of hexanal observed in the dynamic headspace of water samples (SML: dashed lines, bulk: solid lines) obtained from the Sessvoldtjern, Tjernsrudtjern, and Tennungen lakes upon 3-hour exposure to UV, UV and $O_3$, and $O_3$, respectively.

The emission of hexanal during exposure to 0.68 W $m^{-2}$ is about the same level as the emission during 0.2 W $m^{-2}$ exposure, and the 0.35 and 0.10 W $m^{-2}$ exposures have lower emissions of hexanal (see Figure 30).

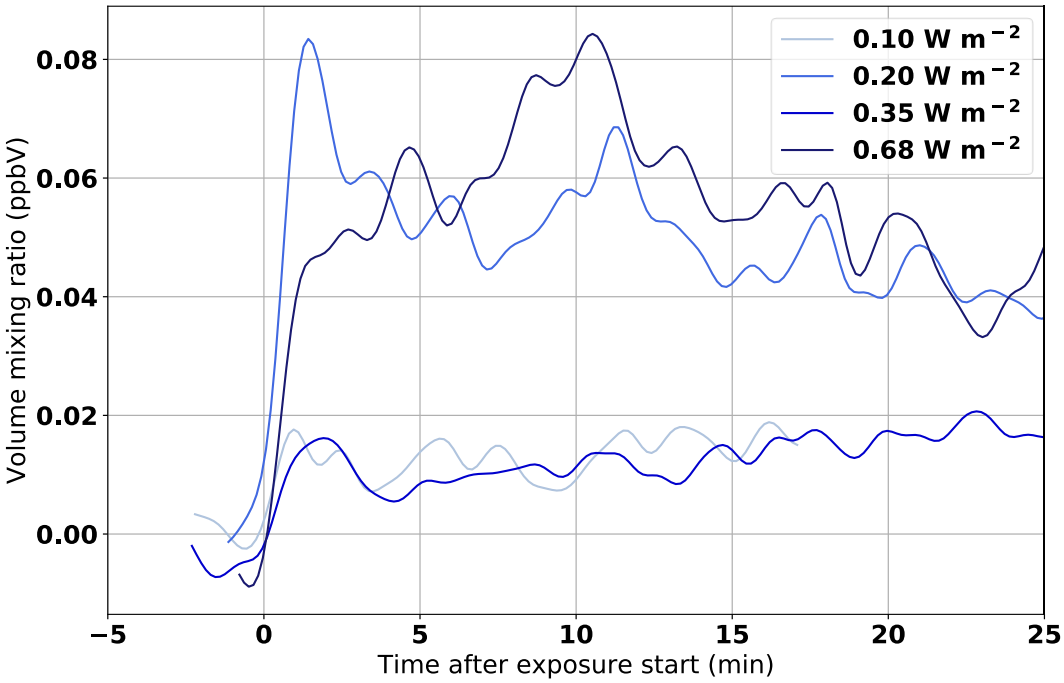


Figure 30. Volume mixing ratios of hexanal observed in the dynamic headspace of water samples obtained from the Tjernsrudtjern lake upon exposure to different UV light intensities.

The emission of hexanal was generally similar between the unfiltered and filtered samples from Svartkulp, but during the UV+$O_3$ exposure the 0.2 µm filtered sample exhibited higher emissions than the 0.45 µm filtered and unfiltered sample. The latter showed similar emission levels.

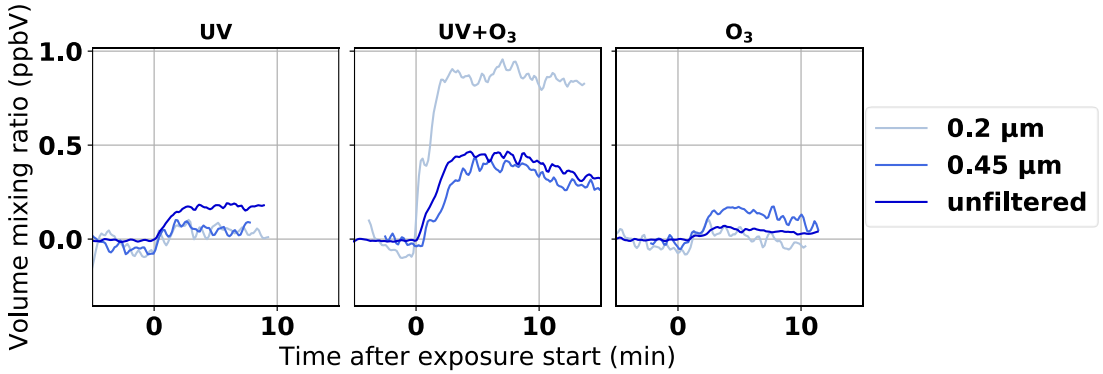


Figure 31. Volume mixing ratios of hexanal observed in the dynamic headspace of filtered (0.2 µm and 0.45 µm) water samples and an unfiltered water sample from the Svartkulp lake upon exposure to UV, UV and $O_3$, and $O_3$, respectively.

The $O_3$-induced emission of hexanal from Tjernsrudtjern, Tennungen and Årungen lake samples may have been formed through ozonolysis of linoleic acid as described by Zhou and co-workers (2014). Svartkulp lake sample exhibits high emissions during exposure to UV+$O_3$,

which could be produced through the photooxidation of carboxylic acids into aldehydes, as suggested by Chiu et al. (2017). A general trend of emissions increasing rapidly before decreasing more slowly was observed, which suggests that there was a reservoir of precursor compounds that get depleted quickly upon exposure to UV and/or $O_3$. The SML did not produce higher emissions of hexanal than the bulk water samples. Higher UV intensities produced higher emissions of hexanal than lower UV intensities, indicating a correlation between UV intensity and emissions.

### 3.2.6 Heptanal

Figure 32 shows the emissions of heptanal (*m/z* 115.11) from each of the lake samples during exposure to UV, UV+$O_3$ and $O_3$ only, respectively.

In Østensjøvann, Kolbotntjern, Årungen and Tennungen the emissions from all three exposures were similar (see Figure 32). Gjersjøen, Tennungen and Tjernsrudtjern emitted the highest volume mixing ratio of heptanal from the $O_3$ condition, while Svartkulp, Lutvann Sværsvann and Sessvoldtjern exhibited their highest emissions when exposed to UV and $O_3$. Generally, the emissions of heptanal were low, only about 50 ppt from most of the lakes, and similar to the background levels.

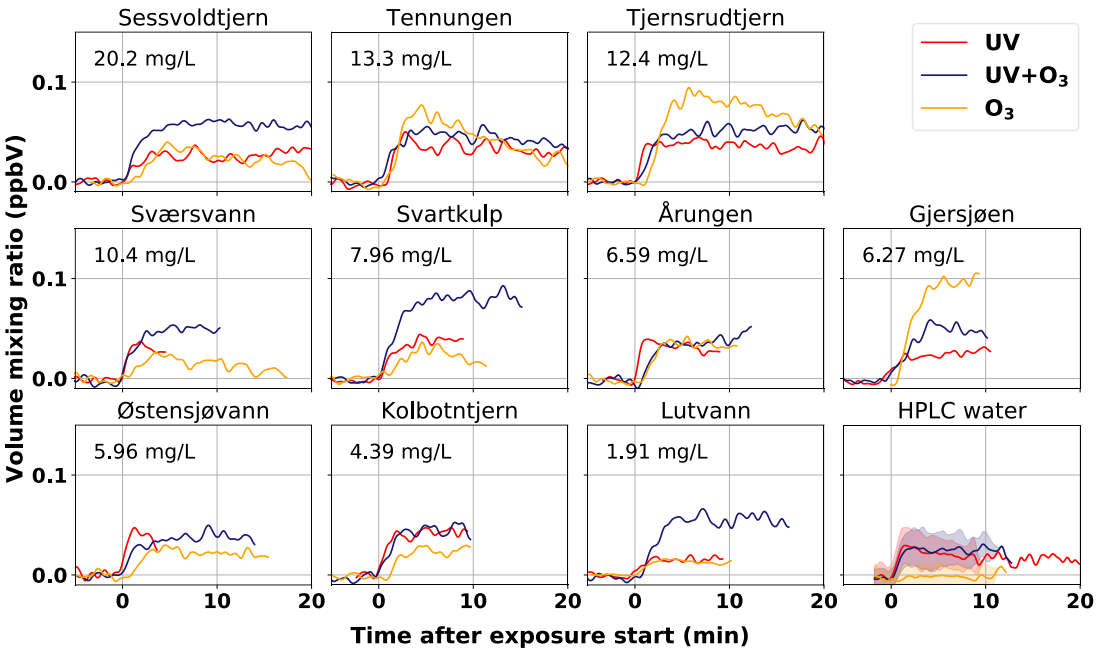


Figure 32. Volume mixing ratios of heptanal observed in the dynamic headspace of water samples obtained from ten Norwegian lakes upon exposure to UV, UV and $O_3$ and $O_3$, respectively. The TOC content of the sample is given in the upper left corner of the subplot. The "HPLC water" subplot shows the mean signal (plus standard deviation in shading) from the HPLC water blank measurements carried out before each measurement.

Heptanal emissions experience a sharp increase in emissions followed by a slower decrease in emissions (see Figure 33). The $O_3$ induced emissions of hexanal decrease to zero, while the UV exposed samples experience a decrease to a constant or very slowly decreasing emission levels.

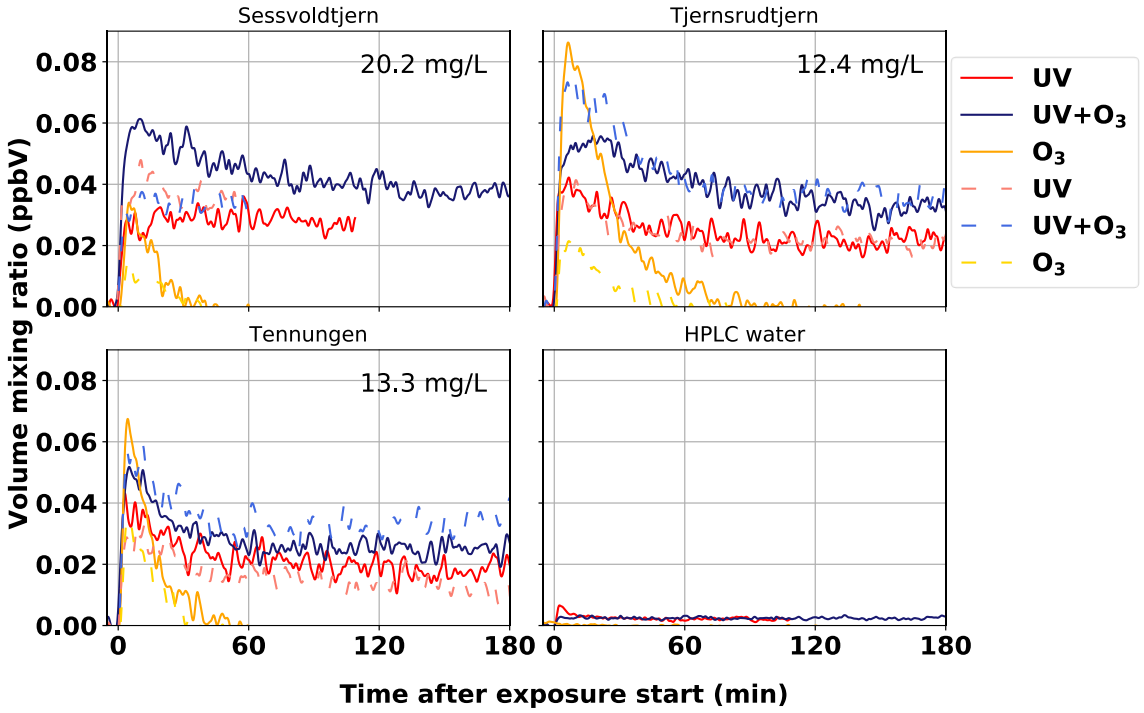


Figure 33. Volume mixing ratios of heptanal observed in the dynamic headspace of water samples (SML: dashed lines, bulk: solid lines) obtained from the Sessvoldtjern, Tjernsrudtjern, and Tennungen lakes upon 3-hour exposure to UV, UV and $O_3$, and $O_3$, respectively.

The 0.68 W $m^{-2}$ exposure caused the highest emission of heptanal, and this is followed by the 0.35 W $m^{-2}$, 0.20 W $m^{-2}$ and 0.10 W $m^{-2}$ exposures which are similar in emission levels (see Figure 34). This suggests that the UV intensity is correlated to the emission of pentanal.

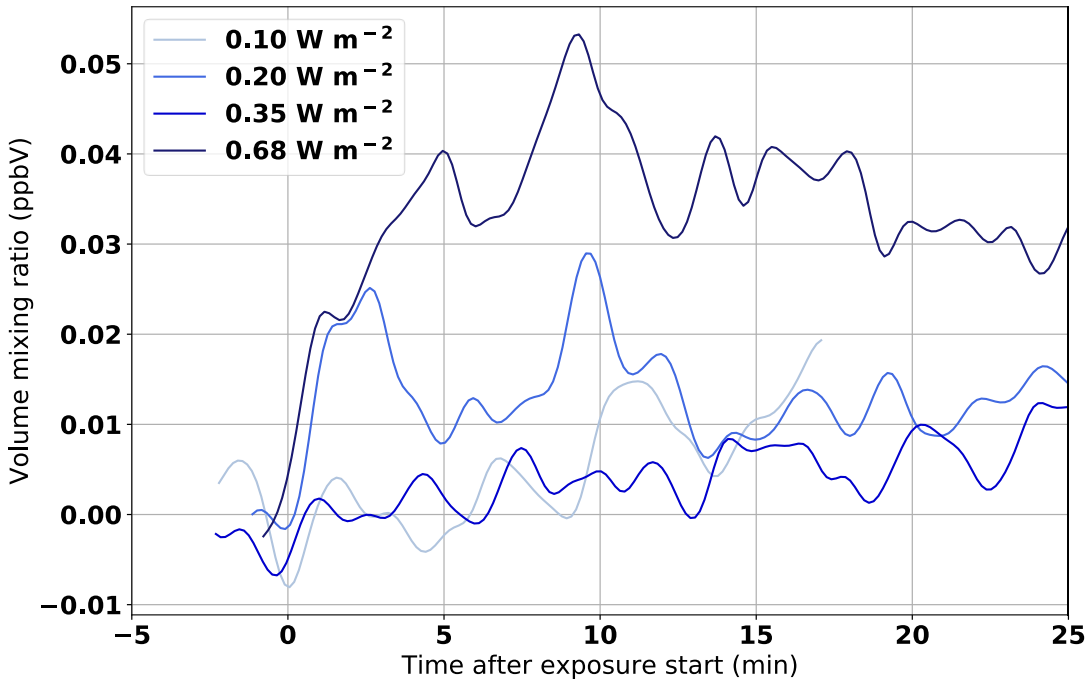


Figure 34. Volume mixing ratios of heptanal observed in the dynamic headspace of water samples obtained from the Tjernsrudtjern lake upon exposure to different UV light intensities.

There are no significant differences between the emissions of heptanal from the filtered and unfiltered samples from Svartkulp (see Figure 35).

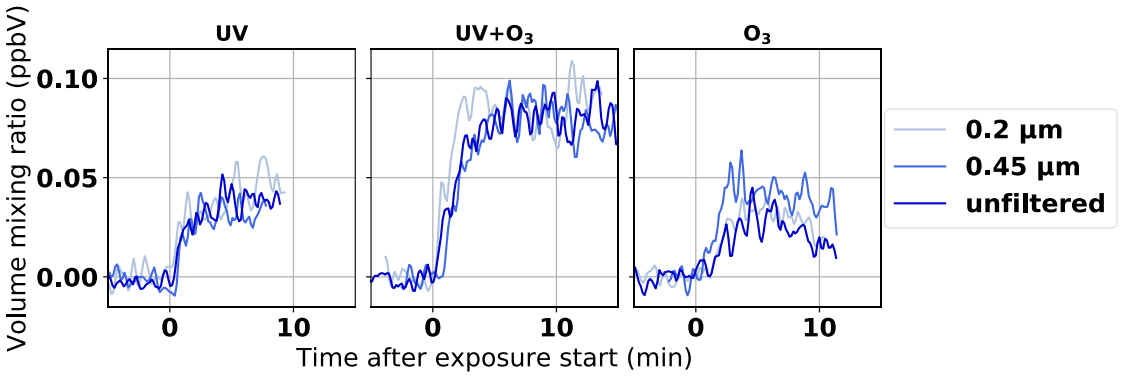


Figure 35. Volume mixing ratios of heptanal observed in the dynamic headspace of filtered (0.2 µm and 0.45 µm) water samples and an unfiltered water sample from the Svartkulp lake upon exposure to UV, UV and $O_3$, and $O_3$, respectively.

The emissions of heptanal are low at around 50 pptV from most lakes, but there were some emissions observed from some lakes during exposure to $O_3$. This suggests the formation of heptanal from ozonolysis, although heptanal was observed from UV exposure in the lakes with high TOC levels.

### 3.2.7 Octanal

Figure 40 shows the emissions of octanal (*m/z* 129.13) from each of the lake samples during exposure to UV, UV+$O_3$ and $O_3$ only, respectively.

Little to no octanal was emitted from the lakes when exposed to $O_3$ (see Figure 36). In the UV and UV+$O_3$ conditions there were some variations in the emissions between the lakes. Østensjøvann, Årungen and Tjernsrudtjern emitted higher volume mixing ratios of octanal during the UV exposure than in the UV+$O_3$ exposure, and the UV induced emissions decrease more quickly than the emissions in the UV+$O_3$ exposure.

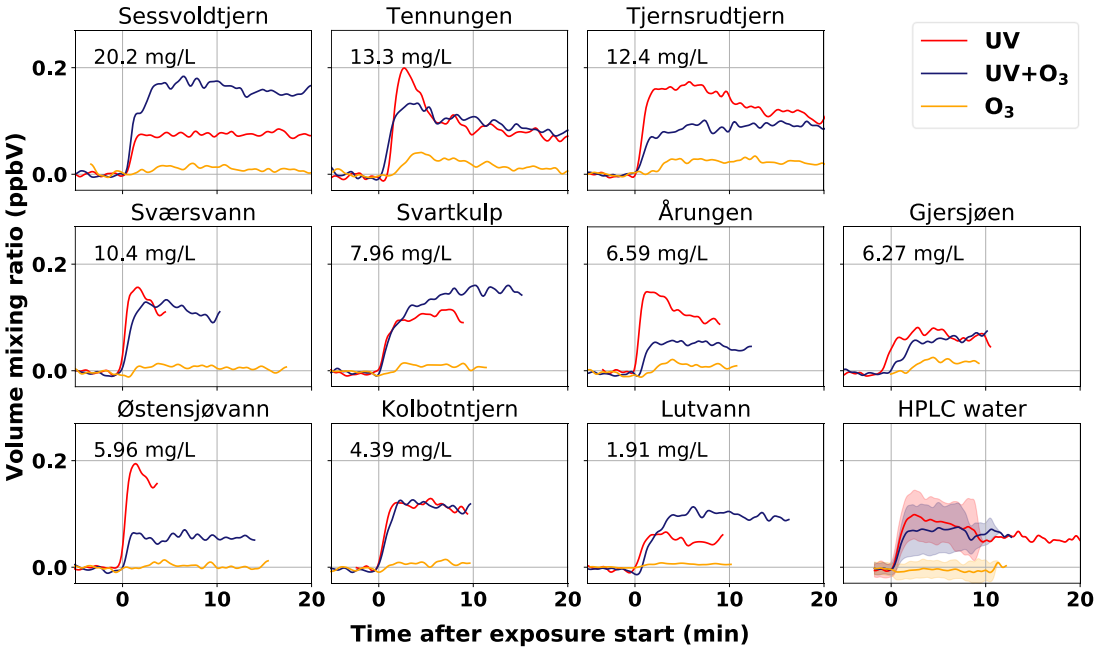


Figure 36. Volume mixing ratios of octanal observed in the dynamic headspace of water samples obtained from ten Norwegian lakes upon exposure to UV, UV and $O_3$ and $O_3$, respectively. The TOC content of the sample is given in the upper left corner of the subplot. The "HPLC water" subplot shows the mean signal (plus standard deviation in shading) from the HPLC water blank measurements carried out before each measurement.

The emissions of octanal increased rapidly before slowly decreasing (see Figure 37). In Sessvoldtjern during the UV+$O_3$ exposure the SML sample emitted about 0.05 ppbV octanal compared to 0.15 ppbV from the bulk sample. The rest of the lakes and exposures have similar octanal emissions from the SML samples and bulk water samples.

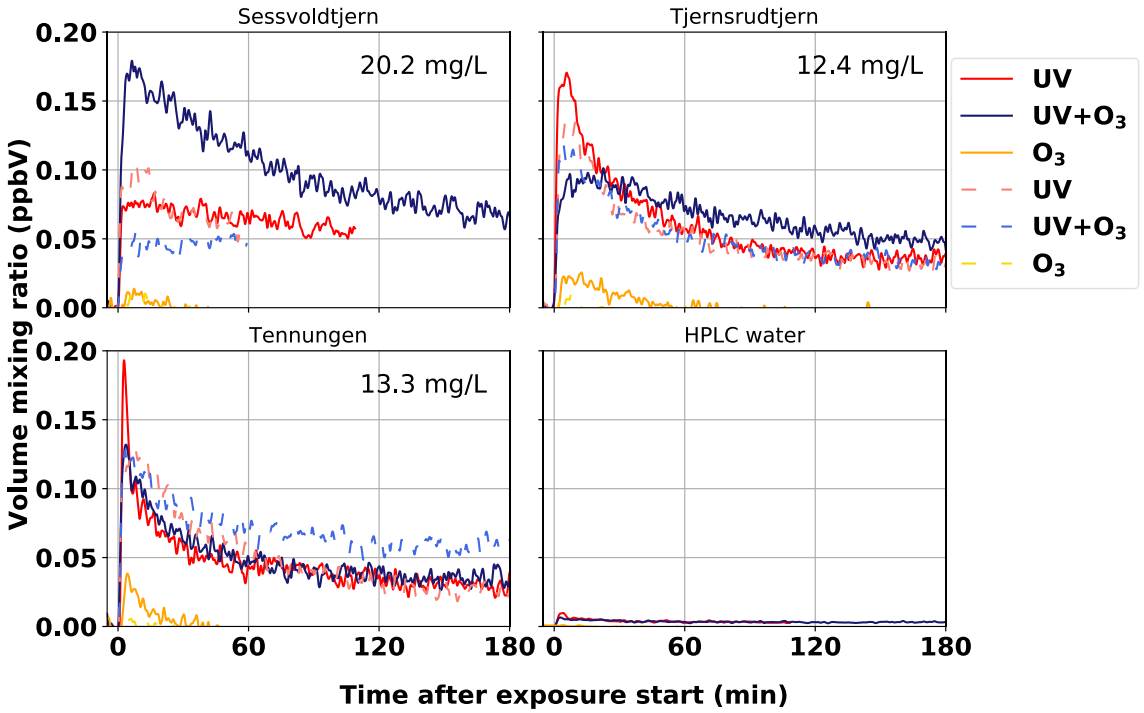


Figure 37. Volume mixing ratios of octanal observed in the dynamic headspace of water samples (SML: dashed lines, bulk: solid lines) obtained from the Sessvoldtjern, Tjernsrudtjern, and Tennungen lakes upon 3-hour exposure to UV, UV and $O_3$, and $O_3$, respectively.

The 0.68 W $m^{-2}$ exposure caused the highest emission of octanal, and was followed by the 0.20 W $m^{-2}$, 0.35 W $m^{-2}$ and 0.10 W $m^{-2}$ exposures respectively. The 0.35 W $m^{-2}$ and 0.10 W $m^{-2}$ exposures caused similar in emission levels (see Figure 38).

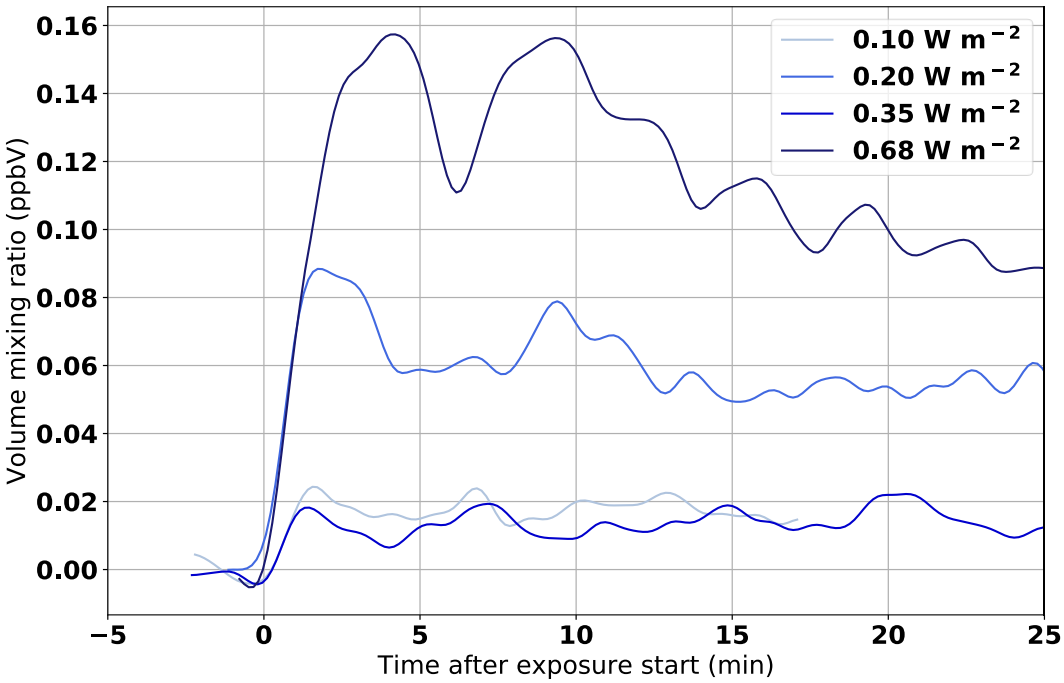


Figure 38. Volume mixing ratios of octanal observed in the dynamic headspace of water samples obtained from the Tjernsrudtjern lake upon exposure to different UV light intensities.

No significant differences between the emissions of octanal from the filtered and unfiltered samples from Svartkulp were observed (see Figure 39).

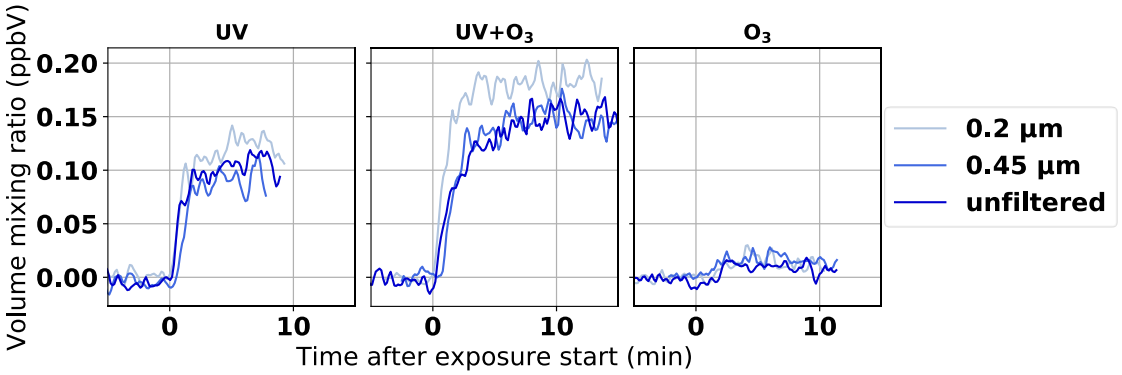


Figure 39. Volume mixing ratios of octanal observed in the dynamic headspace of filtered (0.2 µm and 0.45 µm) water samples and an unfiltered water sample from the Svartkulp lake upon exposure to UV, UV and $O_3$, and $O_3$, respectively.

In general, the emissions of octanal are low relative to the blank measurement, and mainly driven by UV radiation. $O_3$ did not contribute to the formation of octanal. The emissions experienced a rapid increase followed by a slower decrease, indicating that the precursors to octanal are a limited source. Since there are no significant differences between the filtered and unfiltered samples analyzed, the emissions of octanal are expected to be from abiotic sources. Octanal is not produced at a higher level in the SML sample than the bulk water sample.

### 3.2.8 Nonanal

Figure 40 shows the emissions of nonanal (*m/z* 143.14) from each of the lake samples during exposure to UV, UV+$O_3$ and $O_3$ only, respectively.

Nonanal was the compound with the highest overall emissions out of all the compounds we have observed in the first 20 minutes of exposure. Nonanal was emitted in all three exposures in almost all the lakes. The highest emissions were during the $O_3$ exposure from Tennungen, Tjernsrudtjern and Gjersjøen lake samples, as well as the UV+$O_3$ conditions from Svartkulp and Lutvann. All these reach 1 ppb within the first 10 minutes of exposure. The Tennungen and Tjernsrudtjern $O_3$ induced nonanal emissions decay quite quickly compared to most of the other traces. The emissions observed increase before decreasing slowly.

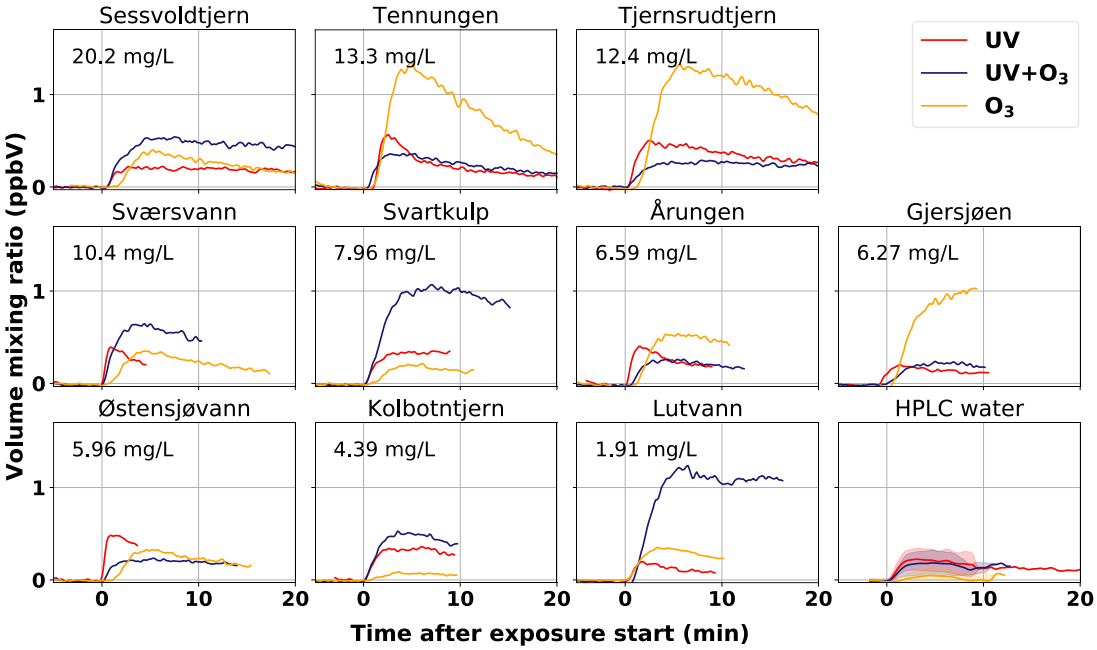


Figure 40. Volume mixing ratios of nonanal observed in the dynamic headspace of water samples obtained from ten Norwegian lakes upon exposure to UV, UV and $O_3$ and $O_3$, respectively. The TOC content of the sample is given in the upper left corner of the subplot. The "HPLC water" subplot shows the mean signal (plus standard deviation in shading) from the HPLC water blank measurements carried out before each measurement.

The three hour exposure shows that the $O_3$ induced emissions rapidly decrease to zero, while the UV and UV+$O_3$ induced emissions decrease and then stabilize at a low emission level (see Figure 41).

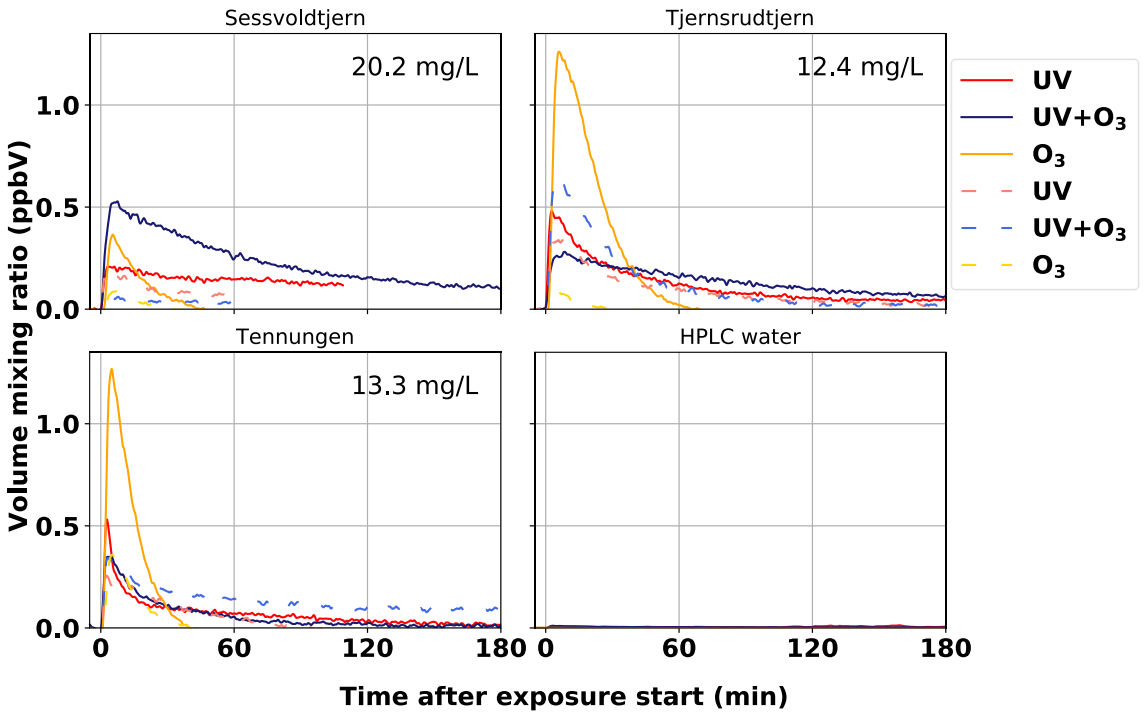


Figure 41. Volume mixing ratios of nonanal observed in the dynamic headspace of water samples (SML: dashed lines, bulk: solid lines) obtained from the Sessvoldtjern, Tjernsrudtjern, and Tennungen lakes upon 3-hour exposure to UV, UV and $O_3$, and $O_3$, respectively.

The 0.68 W $m^{-2}$ exposure caused the highest emission of nonanal, and this is followed by the 0.20 W $m^{-2}$, 0.35 W $m^{-2}$ and 0.10 W $m^{-2}$ exposures respectively. The 0.35 W $m^{-2}$ and 0.10 W $m^{-2}$ exposured caused similar in emission levels (see Figure 42).

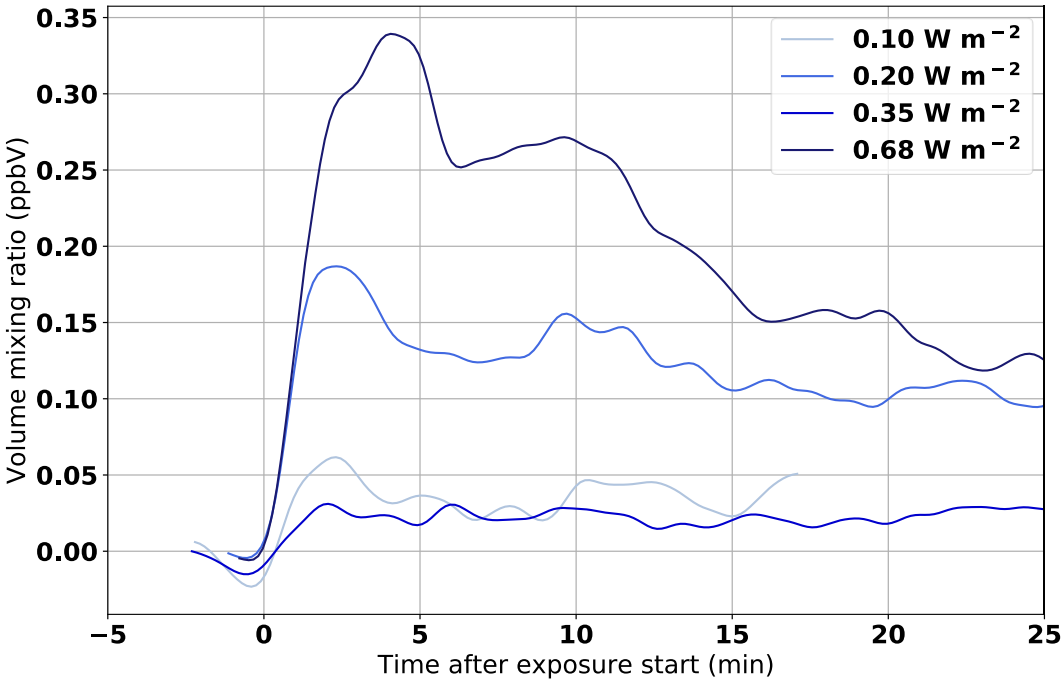


Figure 42. Volume mixing ratios of nonanal observed in the dynamic headspace of water samples obtained from the Tjernsrudtjern lake upon exposure to different UV light intensities.

The emissions from the filtered and unfiltered Svartkulp samples are quite similar, although the 0.2 µm filtered sample is slightly higher than the 0.45 µm filtered and unfiltered samples in all three exposures.

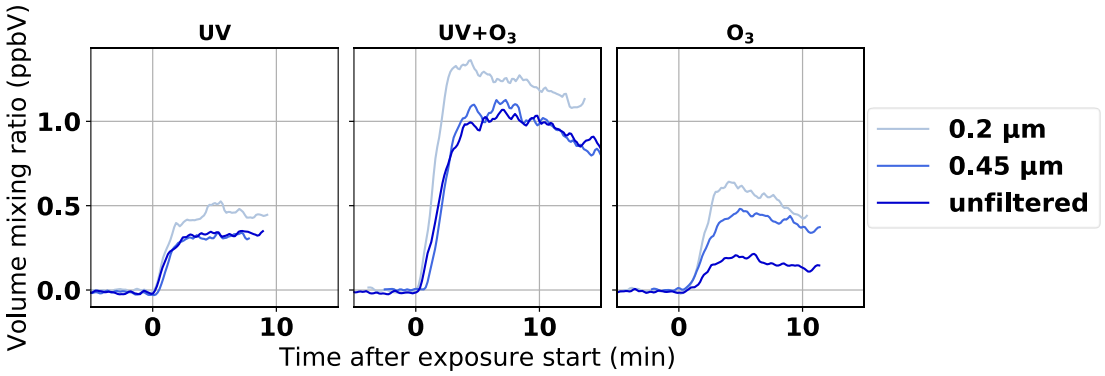


Figure 43. Volume mixing ratios of nonanal observed in the dynamic headspace of filtered (0.2 µm and 0.45 µm) water samples and an unfiltered water sample from the Svartkulp lake upon exposure to UV, UV and $O_3$, and $O_3$, respectively.

The high emissions from UV+$O_3$ and $O_3$ exposures indicated that nonanal was formed largely by ozonolysis in some of the lakes, and possibly in reactions that require both UV radiation and $O_3$. The nonanal may have been produced through photooxidation or ozonolysis of oleic acid or linoleic acid as proposed by Zhou et al. (2014) and Kieber, Hydro, and Seaton (1997).

A significant difference in the emission of nonanal from the SML samples and the bulk water samples was not observed. There was no significant difference between the nonanal emissions from the filtered and unfiltered samples, suggesting that the nonanal emissions observed derive from chemical sources. A correlation between UV intensity and nonanal emissions was observed.

### 3.2.9 Decanal

The emissions of decanal during the short-term exposure to UV, UV and $O_3$ and $O_3$ is shown in Figure 44. The emission of decanal was low from most lakes and exposures, but the UV+$O_3$ exposure in Svartkulp and Sværsvann induced emissions up to 0.2 and 0.1 ppbV respectively. Tennungen lake sample emitted decanal upon exposure to $O_3$.

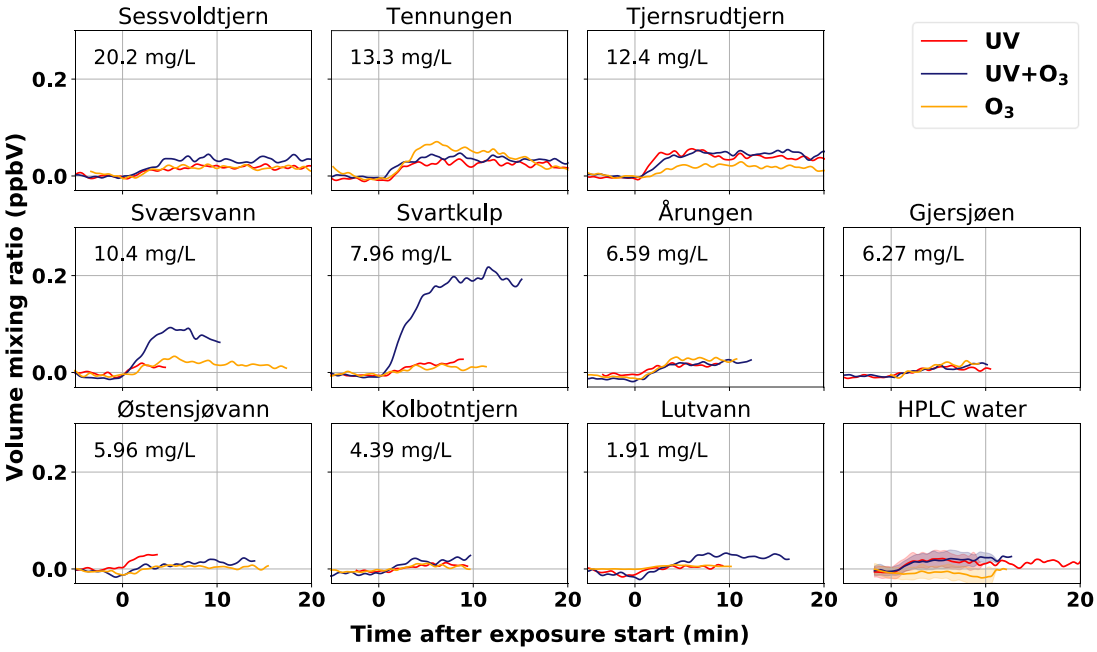


Figure 44. Volume mixing ratios of decanal observed in the dynamic headspace of water samples obtained from ten Norwegian lakes upon exposure to UV, UV and $O_3$ and $O_3$, respectively. The TOC content of the sample is given in the upper left corner of the subplot. The "HPLC water" subplot shows the mean signal (plus standard deviation in shading) from the HPLC water blank measurements carried out before each measurement.

Figure 45 shows the emission of decanal during 3 hour exposure to UV, UV and $O_3$ and $O_3$, respectively from Sessvoldtjern, Tjernsrudtjern and Tennungen samples. The Sessvoldtjern lake sample exhibited stable emissions of decanal during 3 hours of exposure to UV and

UV+$O_3$, while Tjernsrudtjern and Tennungen samples experienced a slow decrease in emissions. The decanal emissions from the SML samples were mostly similar to the emissions from the bulk water, but the Tjernsrudtjern SML sample emitted slightly lower levels of decanal than the bulk water during exposure to UV and UV+$O_3$. The Sessvoldtjern SML sample also emitted lower levels of decanal than the bulk sample during UV+$O_3$ exposure.

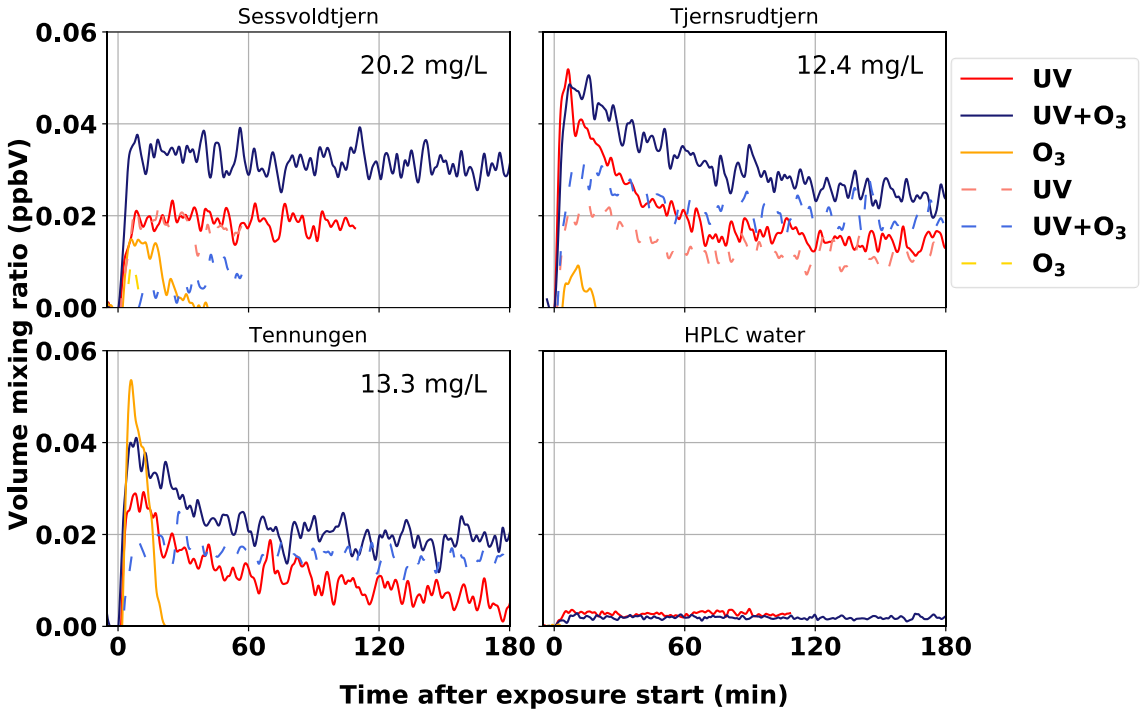


Figure 45. Volume mixing ratios of decanal observed in the dynamic headspace of water samples (SML: dashed lines, bulk: solid lines) obtained from the Sessvoldtjern, Tjernsrudtjern, and Tennungen lakes upon 3-hour exposure to UV, UV and $O_3$, and $O_3$, respectively.

Figure 46 shows the emission of decanal during exposure to UV light of varying intensity. No increase in the emission of decanal was observed in this figure.

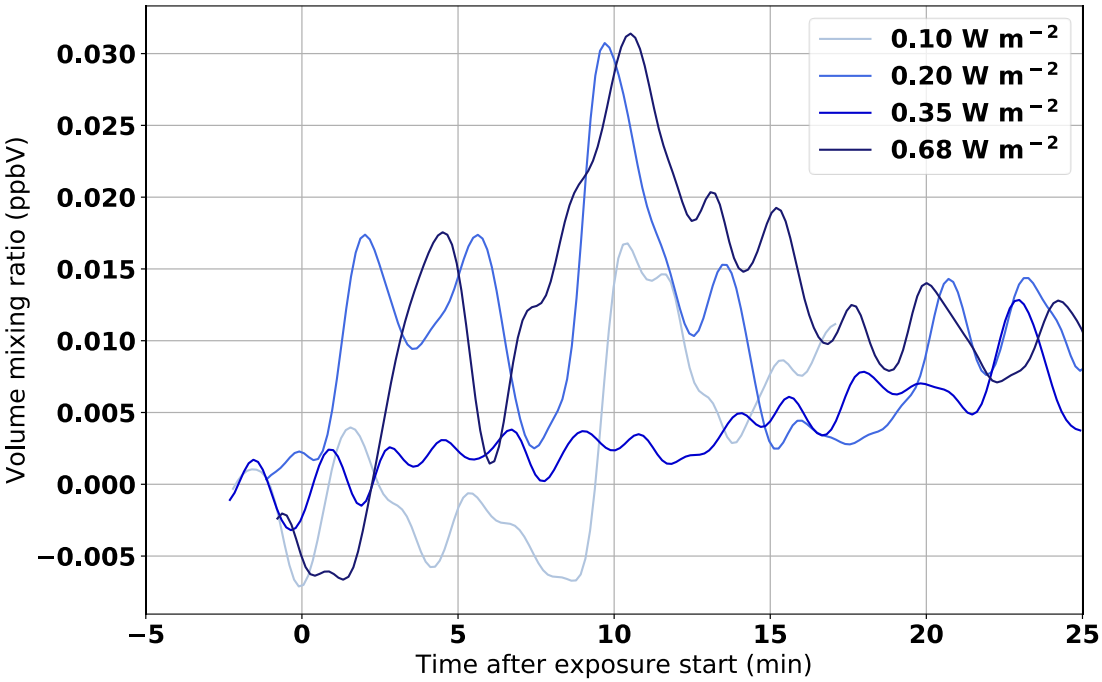


Figure 46. Volume mixing ratios of decanal observed in the dynamic headspace of water samples obtained from the Tjernsrudtjern lake upon exposure to different UV light intensities.

The emission of decanal from filtered and unfiltered samples are shown in Figure 47. There were no observed differences in the emission of decanal during the UV and $O_3$ exposures, but during the UV+$O_3$ exposure the unfiltered sample emits twice the amount that the two filtered samples do.

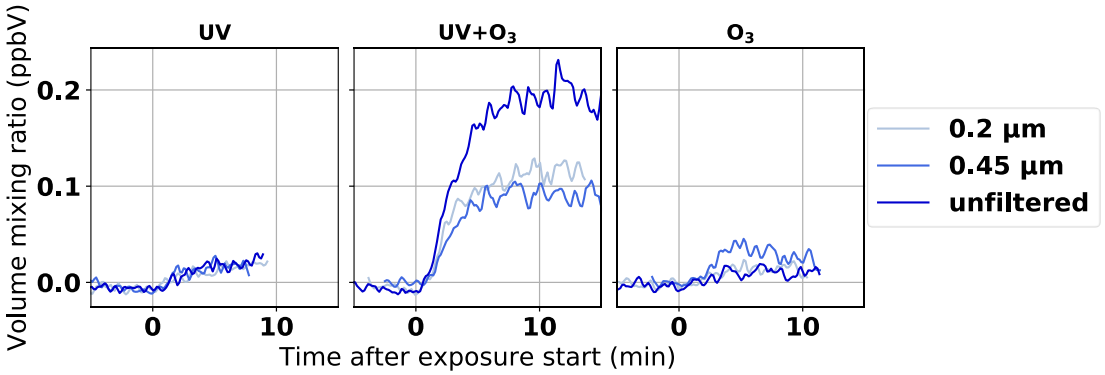


Figure 47. Volume mixing ratios of decanal observed in the dynamic headspace of filtered (0.2 µm and 0.45 µm) water samples and an unfiltered water sample from the Svartkulp lake upon exposure to UV, UV and $O_3$, and $O_3$, respectively.

Emissions of decanal significantly higher than background was observed from Svartkulp and Sværsvann samples exposed to UV+$O_3$ and Tennungen exposed to $O_3$. The emissions from Svartkulp and Sværsvann may be produced through photooxidation and ozonolysis of carboxylic acids by the mechanism shown in Figure 1 (Chiu et al. 2017). The decanal emitted from Tennungen upon exposure to $O_3$ may have been produced through the ozonolysis of polyunsaturated carboxylic acids as shown in Figure 3 (Zhou et al. 2014)

### 3.2.10 Undecanal

The emissions of undecanal during exposure to UV, UV+$O_3$ and $O_3$ were low and not significantly higher than background levels observed from the blank (see Figure 48). Svartkulp exposed to UV+$O_3$ potentially had emissions increasing to levels higher than that observed from the HPLC water blank, but the measurement was stopped before the levels stabilized. Figure 49 shows the undecanal emissions from Sessvoldtjern, Tjernsrudtjern and Tennungen when exposed to UV, UV+$O_3$ and $O_3$ for three hours.

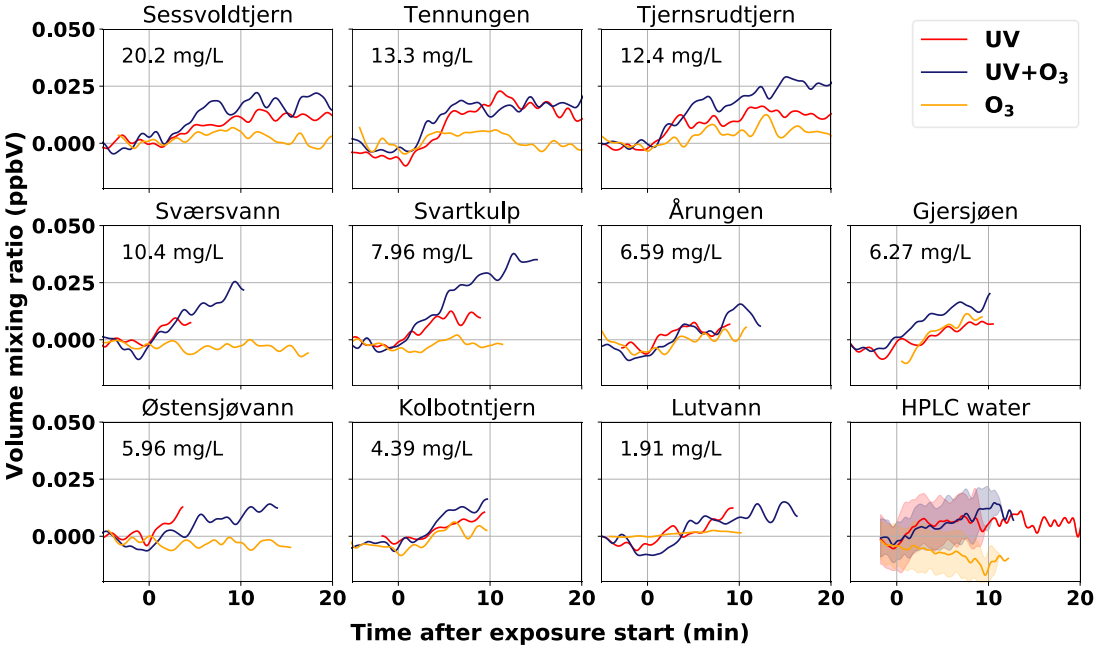


Figure 48. Volume mixing ratios of undecanal observed in the dynamic headspace of water samples obtained from ten Norwegian lakes upon exposure to UV, UV and $O_3$ and $O_3$, respectively. The TOC content of the sample is given in the upper left corner of the subplot. The "HPLC water" subplot shows the mean signal (plus standard deviation in shading) from the HPLC water blank measurements carried out before each measurement.

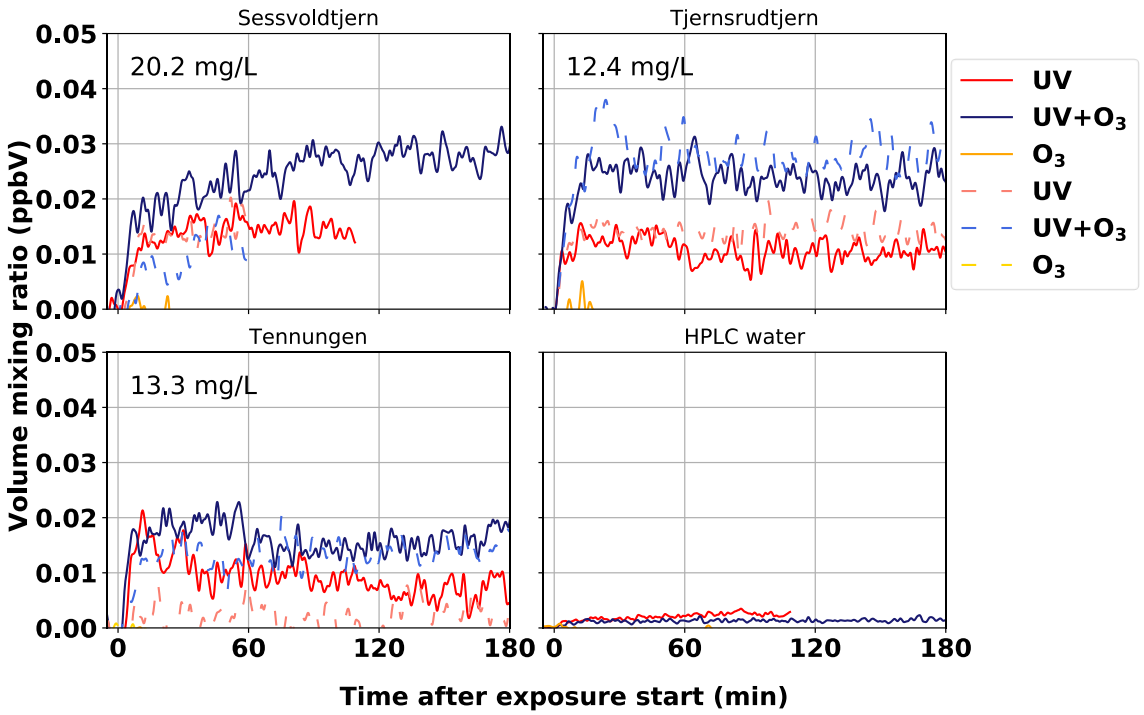


Figure 49. Volume mixing ratios of undecanal observed in the dynamic headspace of water samples (SML: dashed lines, bulk: solid lines) obtained from the Sessvoldtjern, Tjernsrudtjern, and Tennungen lakes upon 3-hour exposure to UV, UV and $O_3$, and $O_3$, respectively.

Figure 50 shows the emitted undecanal during exposure to different UV intensities, and there was no trend observed in these emissions as the emissions were close to the background and have high noise levels.

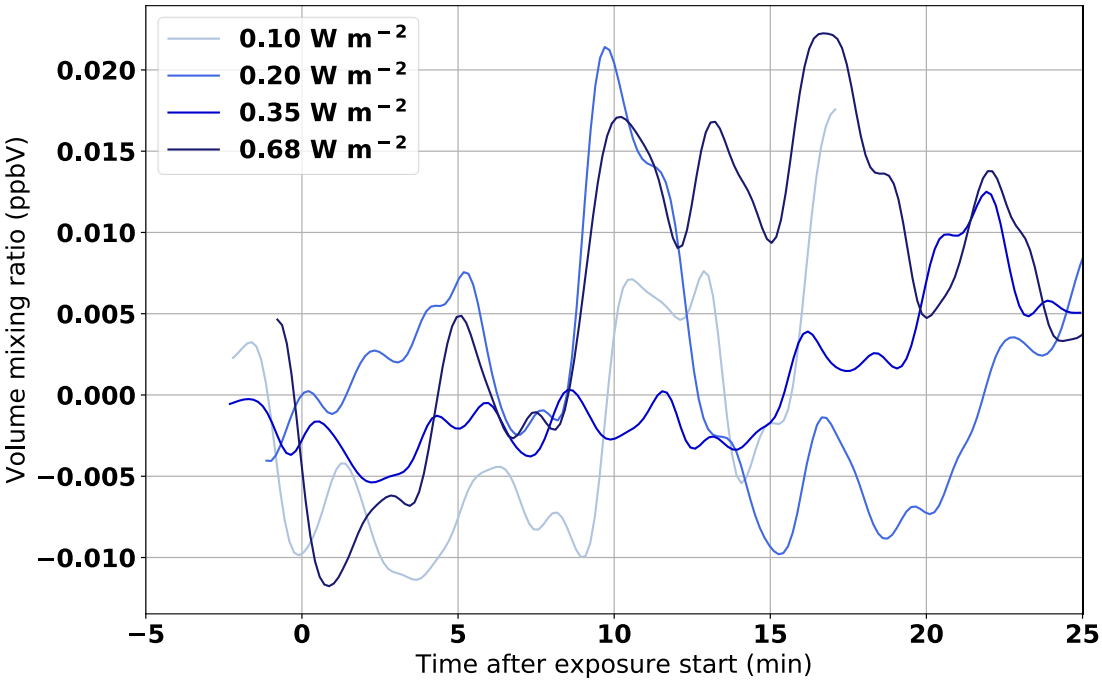


Figure 50. Volume mixing ratios of undecanal observed in the dynamic headspace of water samples obtained from the Tjernsrudtjern lake upon exposure to different UV light intensities.

There is no perceivable difference in the emission of undecanal between the filtered and unfiltered samples from Svartkulp (see Figure 51).

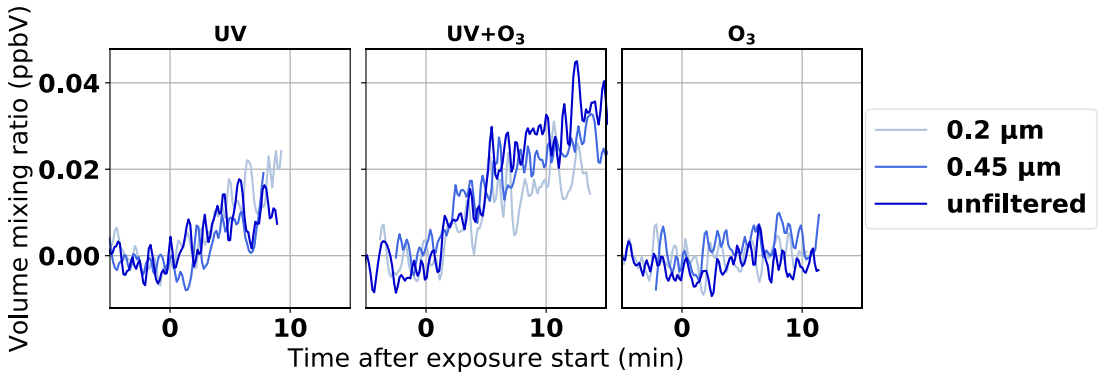


Figure 51. Volume mixing ratios of undecanal observed in the dynamic headspace of filtered (0.2 µm and 0.45 µm) water samples and an unfiltered water sample from the Svartkulp lake upon exposure to UV, UV and $O_3$, and $O_3$, respectively.

The emissions observed from the samples were similar to the background levels. From the evidence presented it cannot be concluded that undecanal was emitted from the lakes studied at a significant rate.

### 3.2.11 Pentadecene and heptadecene

The signals at m/z 211.24 and m/z 239.27 were tentatively assigned to pentadecene and heptadecene, respectively.

In the short-term exposure experiments, the signals assigned to the two unsaturated long-chain hydrocarbons were clearly above the HPLC water blank levels only for Tjernsrudtjern sample upon exposure to UV and $O_3$ (Figures 52 and 53). The Tjernsrudtjern sample was also the only one that exhibited a significant increase in pentadecene and heptadecene emissions in the 3-hour exposure experiments (Figures 54 and 55). The strong increase was only observed in the bulk water samples upon exposure to UV+$O_3$ and to a lesser extent upon exposure to UV light only. Volume mixing ratios below 0.1 ppbV are similar to those found in the HPLC water blank (Figures 54 and 55) and are thus not considered being significant.

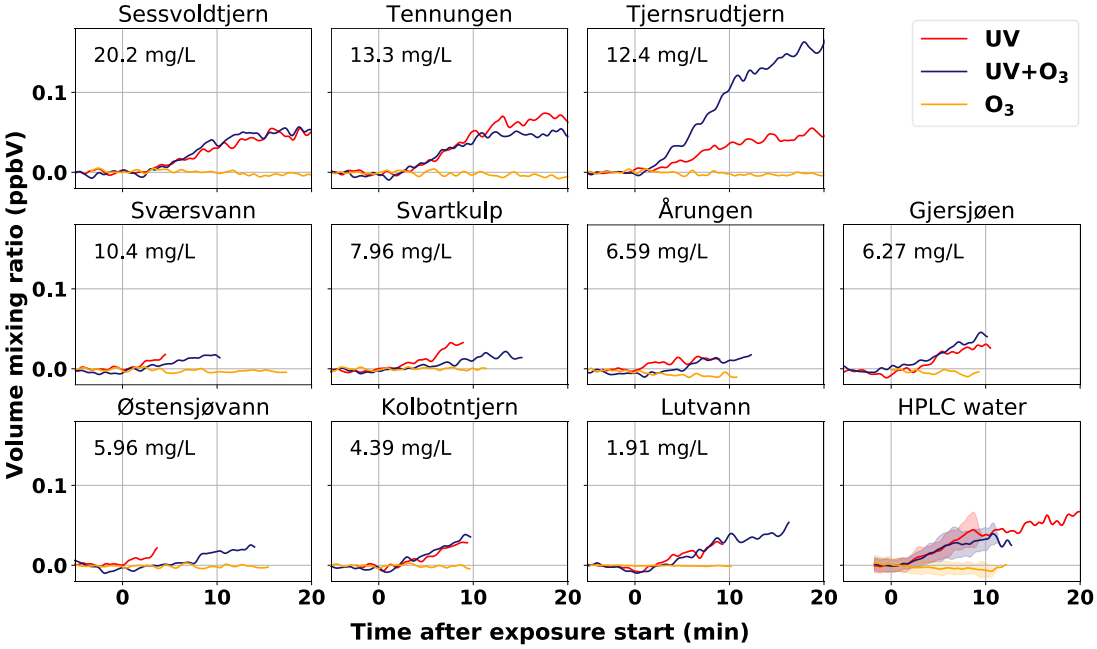


Figure 52. Volume mixing ratios of pentadecene observed in the dynamic headspace of water samples obtained from ten Norwegian lakes upon exposure to UV, UV and $O_3$ and $O_3$, respectively. The TOC content of the sample is given in the upper left corner of the subplot. The "HPLC water" subplot shows the mean signal (plus standard deviation in shading) from the HPLC water blank measurements carried out before each measurement.

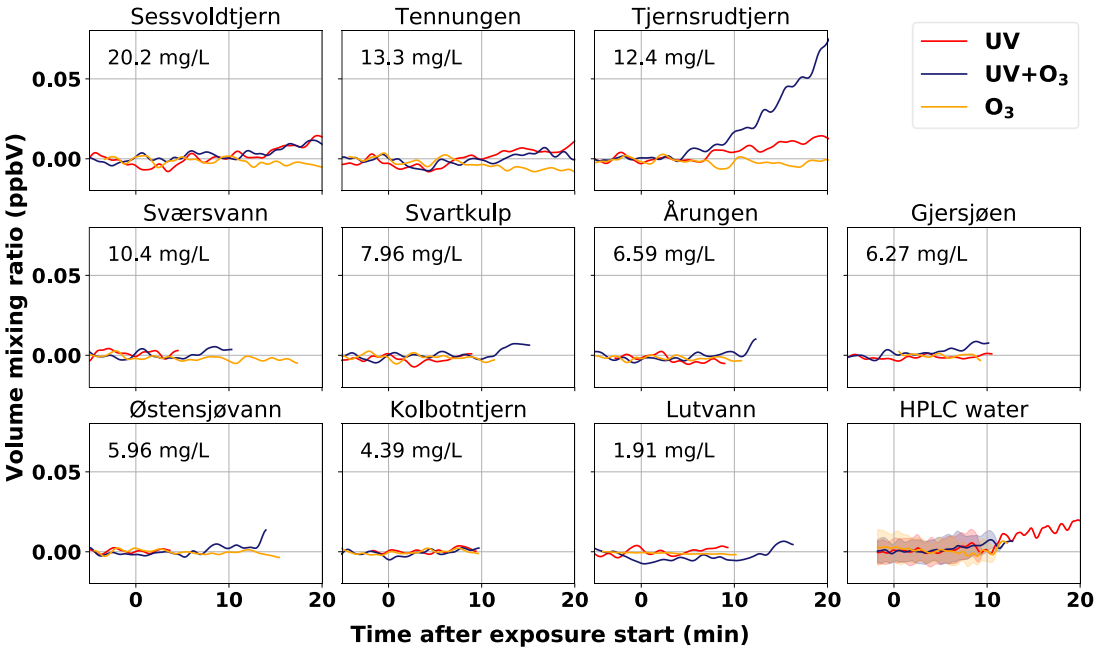


Figure 53. Volume mixing ratios of heptadecene observed in the dynamic headspace of water samples obtained from ten Norwegian lakes upon exposure to UV, UV and $O_3$ and $O_3$, respectively. The TOC content of the sample is given in the upper left corner of the subplot. The "HPLC water" subplot shows the mean signal (plus standard deviation in shading) from the HPLC water blank measurements carried out before each measurement.

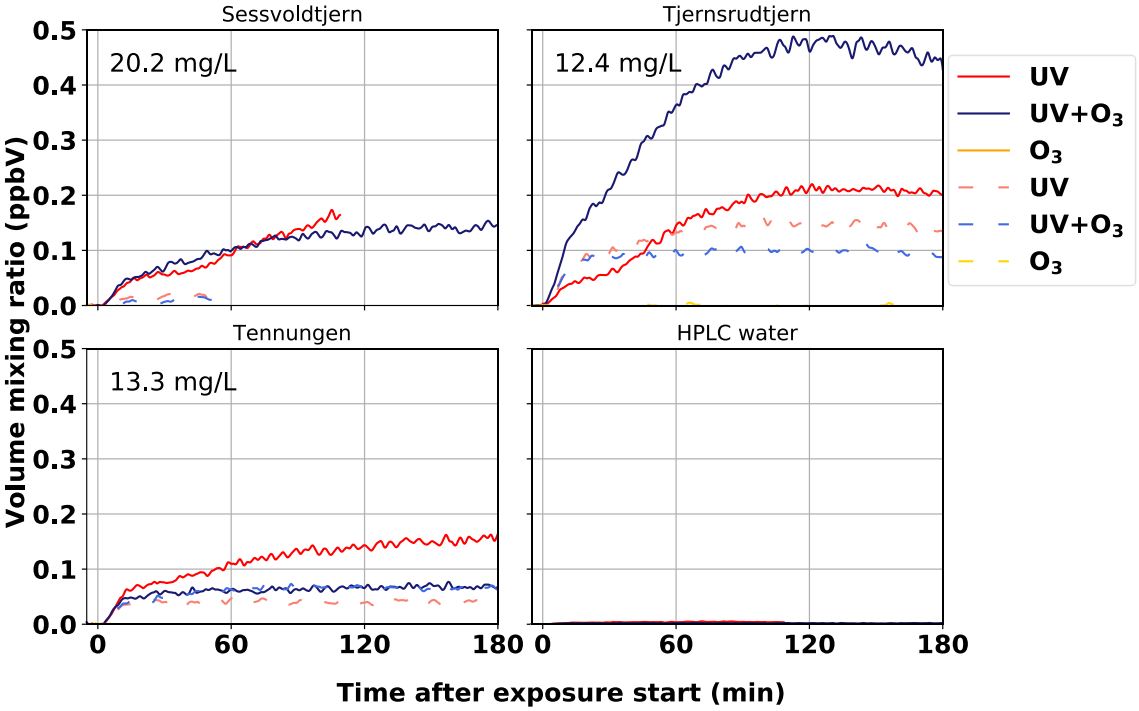


Figure 54. Volume mixing ratios of pentadecene observed in the dynamic headspace of water samples (SML: dashed lines, bulk: solid lines) obtained from the Sessvoldtjern, Tjernsrudtjern, and Tennungen lakes upon 3-hour exposure to UV, UV and $O_3$, and $O_3$, respectively.

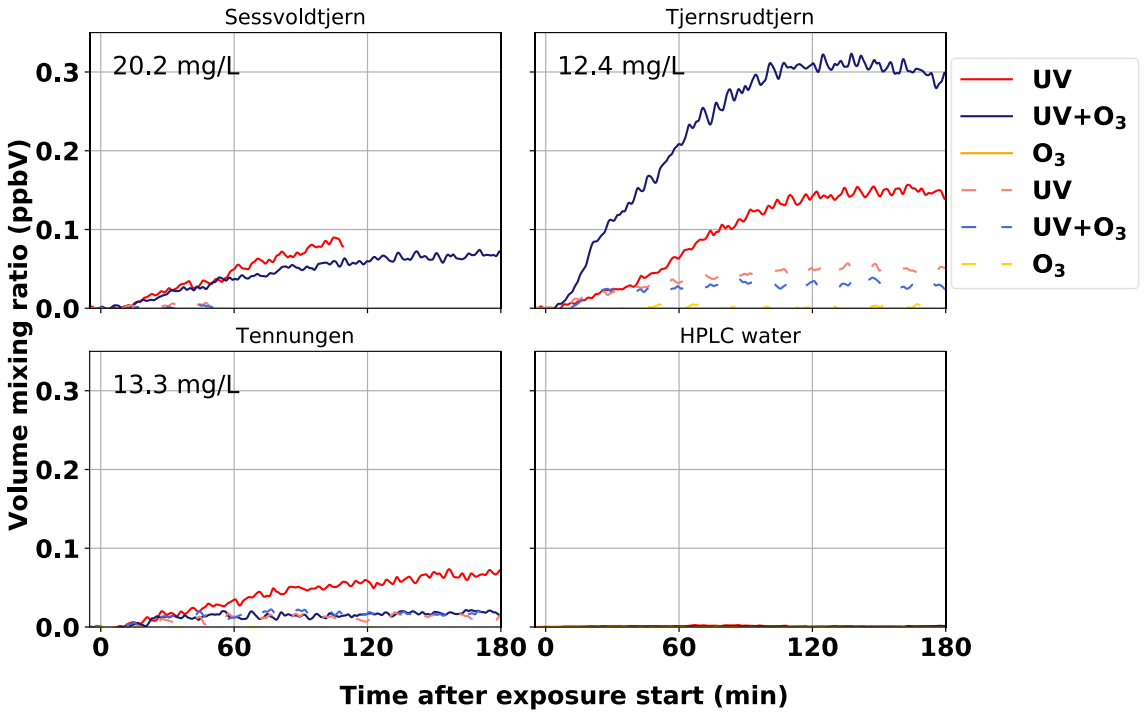


Figure 55. Volume mixing ratios of heptadecene observed in the dynamic headspace of water samples (SML: dashed lines, bulk: solid lines) obtained from the Sessvoldtjern, Tjernsrudtjern, and Tennungen lakes upon 3-hour exposure to UV, UV and $O_3$, and $O_3$, respectively.

The UV variation experiments only lasted for 25 minutes, which was not long enough for investigating any effects on pentadecene and heptadecene emissions. Though it will not be discussed, the results from the UV variation experiments are shown in Figures 56-57. No filtration experiments were carried out on the Tjernsrudtjern sample, but the results from the filtration experiment on Svartkulp lake is shown in Figures 58-59. These will not be discussed either as no emissions higher than background was observed from the Svartkulp sample.

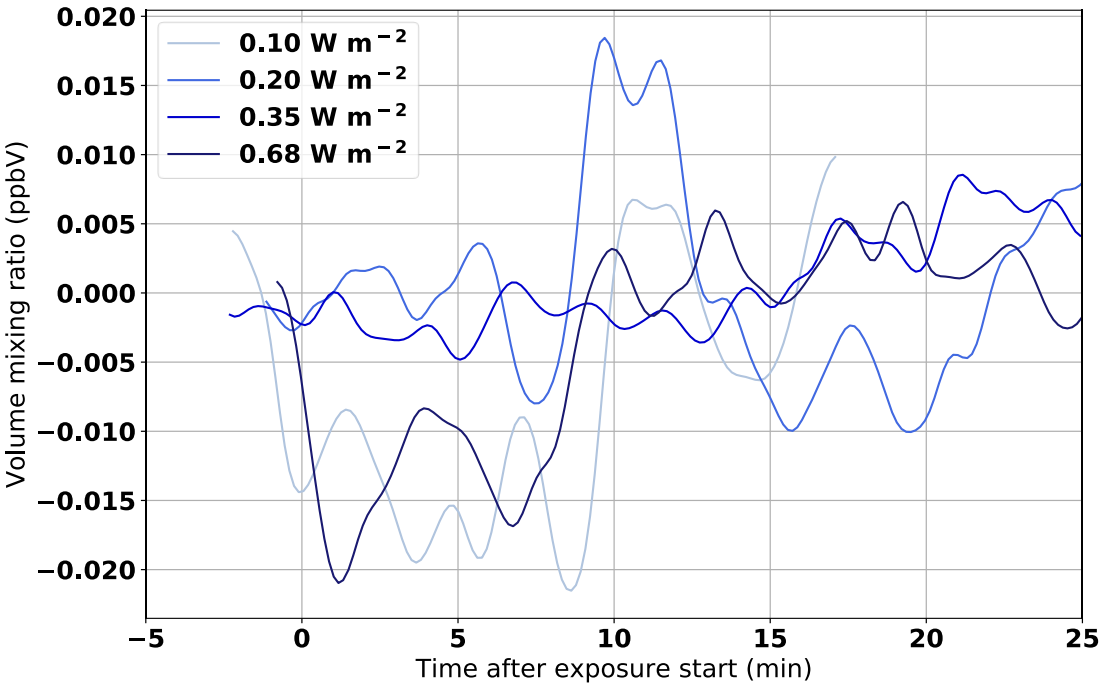


Figure 56. Volume mixing ratios of pentadecene observed in the dynamic headspace of water samples obtained from the Tjernsrudtjern lake upon exposure to different UV light intensities.

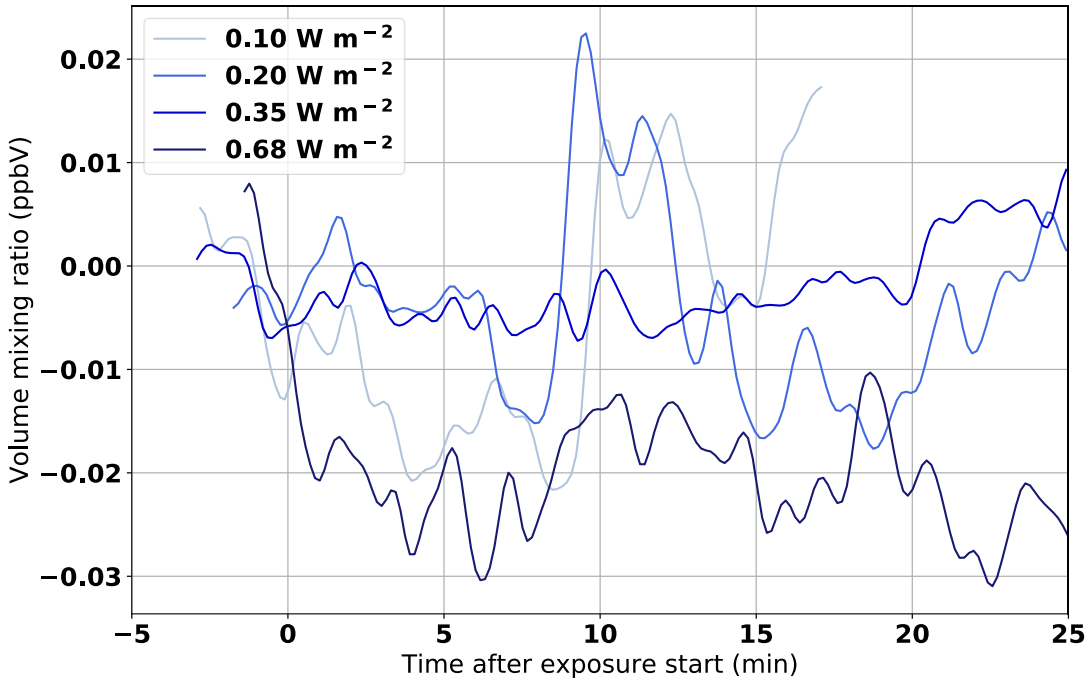


Figure 57. Volume mixing ratios of heptadecene observed in the dynamic headspace of water samples obtained from the Tjernsrudtjern lake upon exposure to different UV light intensities.

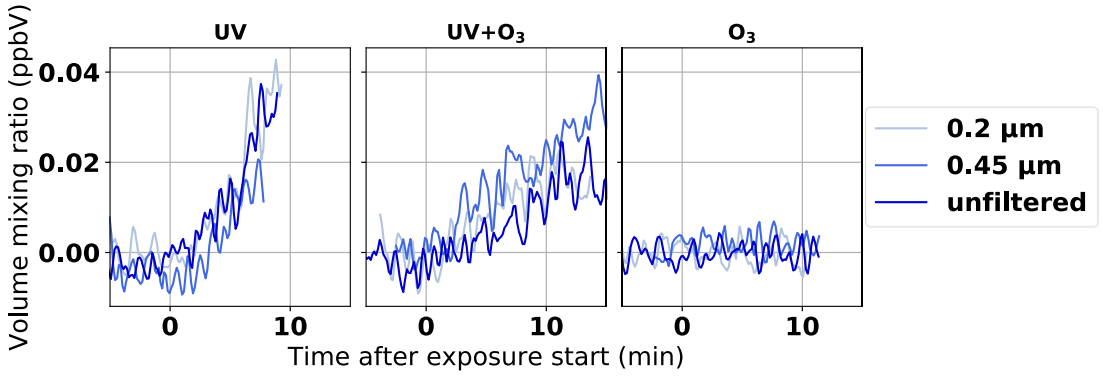


Figure 58. Volume mixing ratios of pentadecene observed in the dynamic headspace of filtered (0.2 µm and 0.45 µm) water samples and an unfiltered water sample from the Svartkulp lake upon exposure to UV, UV and $O_3$, and $O_3$, respectively.

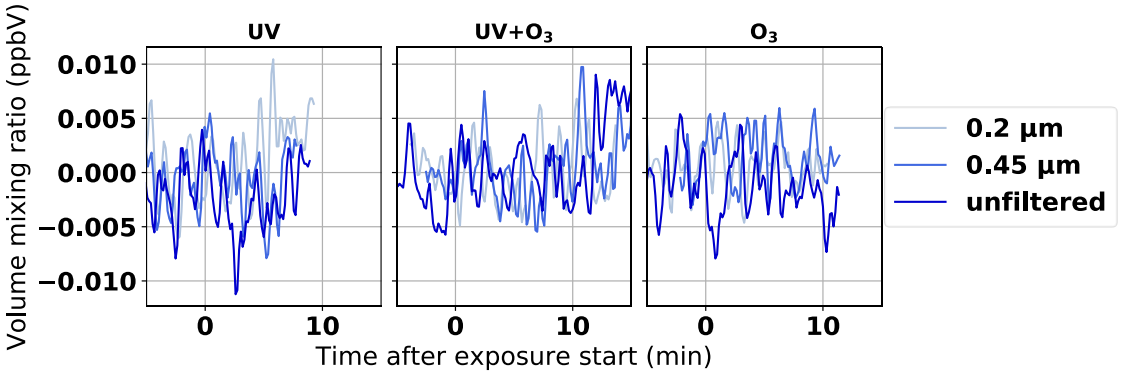


Figure 59. Volume mixing ratios of heptadecene observed in the dynamic headspace of filtered (0.2 µm and 0.45 µm) water samples and an unfiltered water sample from the Svartkulp lake upon exposure to UV, UV and $O_3$, and $O_3$, respectively.

The volume mixing ratios of pentadecene and heptadecene increased slowly, indicating that the formation of these unsaturated hydrocarbons is a slow process. DNOM may be slowly broken down into pentadecene/heptadecene or their precursors. Another potential formation process is the stress-induced release from cyanobacteria in the lake water. Cyanobacteria have been found to produce pentadecene and heptadecene(Zhu et al. 2018), and since cyanobacteria are present in most lakes this could be a formation process for the heptadecene we observed (Vuorio, Järvinen, and Kotamäki 2020; Ininbergs et al. 2011).

# 4 Conclusion

This study investigated the emissions of VOCs from 10 boreal lakes when exposed to UV light and $O_3$. The total organic carbon content of the lakes was measured and the emissions of methanol, acetaldehyde, acetone/propanal, pentanal, hexanal, heptanal, octanal, nonanal, decanal, undecanal, pentadecene and heptadecene were measured during exposure to UV light and ozone, both separately and combined.

Most of the lakes emitted the highest concentrations of VOCs when exposed to UV radiation, which indicates that the compounds observed are mainly formed during photooxidation. A correlation between UV intensity and VOC emission levels was observed for methanol, acetaldehyde, acetone/propanal and $C_5$-$C_9$ aldehydes, but this was only tested on samples from one lake and only included four different UV intensities. With the limited data available a strong conclusion cannot be made, and more experiments are needed to support the evidence.

Compounds such as hexanal and nonanal were emitted at high concentrations during exposure to $O_3$ in four lakes, indicating that these compounds can be formed through ozonolysis, which is supported by the work of Zhou and co-workers (2014). Measurements of sterilized samples showed no differences in emissions of VOCs when compared to unfiltered samples, apart from hexanal and nonanal whose emissions may be inhibited by microorganisms and decanal which may be enhanced by microorganisms. This suggests that the VOC emissions observed were formed through chemical mechanisms, while hexanal, nonanal and decanal emissions may have some contributions from biological sources.

There was a positive correlation between the TOC level in a lake and the emission of VOCs. As lakes in Norway have increasing concentrations of colored organic compounds and TOC, this could lead to higher VOC emissions from lakes in the future (Finstad et al. 2016). This can contribute to changes in the regional climate and affect local air quality. Researching the factors contributing to these changes as well as monitoring the changes is of importance. It is recomended for future work to study the formation mechanism of the compounds observed in this investigation in more detail. The precursors of the VOCs observed are unknown, so studying the origin of the VOC emissions would yield valuable information about how they are formed.

# References

Allesson, Lina, Birgit Koehler, Jan Erik Thrane, Tom Andersen, and Dag O. Hessen. 2021. "The Role of Photomineralization for CO2 Emissions in Boreal Lakes along a Gradient of Dissolved Organic Matter." *Limnology and Oceanography* 66 (1): 158–70. https://doi.org/10.1002/lno.11594.

Anglada, Josep M., Marilia T.C. Martins-Costa, Joseph S. Francisco, and Manuel F. Ruiz-López. 2020. "Photoinduced Oxidation Reactions at the Air-Water Interface." *Journal of the American Chemical Society*. American Chemical Society. https://doi.org/10.1021/jacs.0c06858.

Bernard, F., R. Ciuraru, A. Boréave, and C. George. 2016. "Photosensitized Formation of Secondary Organic Aerosols above the Air/Water Interface." *Environmental Science and Technology* 50 (16): 8678–86. https://doi.org/10.1021/acs.est.6b03520.

Bertilsson, Stefan, Ramunas Stepanauskas, Rocio Cuadros-Hansson, Wilhelm Granéli, Johan Wikner, and Lars Tranvik. 1999. "Photochemically Induced Changes in Bioavailable Carbon and Nitrogen Pools in a Boreal Watershed." *Aquatic Microbial Ecology* 19 (1): 47–56. https://doi.org/10.3354/ame019047.

Carpenter, Lucy J, Stephen D Archer, and Rachael Beale. 2012. "Ocean-Atmosphere Trace Gas Exchange." *Chem. Soc. Rev.* 41 (19): 6473–6506. https://doi.org/10.1039/C2CS35121H.

Chiu, R., L. Tinel, L. Gonzalez, R. Ciuraru, F. Bernard, C. George, and R. Volkamer. 2017. "UV Photochemistry of Carboxylic Acids at the Air-Sea Boundary: A Relevant Source of Glyoxal and Other Oxygenated VOC in the Marine Atmosphere." *Geophysical Research Letters* 44 (2): 1079–87. https://doi.org/10.1002/2016GL071240.

Ciuraru, Raluca, Ludovic Fine, Manuela van Pinxteren, Barbara D'Anna, Hartmut Herrmann, and Christian George. 2015. "Photosensitized Production of Functionalized and Unsaturated Organic Compounds at the Air-Sea Interface." *Scientific Reports* 5 (1): 12741. https://doi.org/10.1038/srep12741.

Cuong, Dang The, Subramanian Karuppiah, and Jeffrey Philip Obbard. 2008. "Distribution of Heavy Metals in the Dissolved and Suspended Phase of the Sea-Surface Microlayer, Seawater Column and in Sediments of Singapore's Coastal Environment." *Environmental*

*Monitoring and Assessment* 138 (1–3): 255–72. https://doi.org/10.1007/s10661-007-9795-y.

Dean, Walter E. 1998. "Magnitude and Significance of Carbon Burial in Lakes, Reservoirs, and Peatlands." http://conservancy.umn.edu/handle/11299/151367.

Drake, Travis W., Peter A. Raymond, and Robert G. M. Spencer. 2018. "Terrestrial Carbon Inputs to Inland Waters: A Current Synthesis of Estimates and Uncertainty." *Limnology and Oceanography Letters* 3 (3): 132–42. https://doi.org/10.1002/lol2.10055.

Ebling, Alina M., and William M. Landing. 2015. "Sampling and Analysis of the Sea Surface Microlayer for Dissolved and Particulate Trace Elements." *Marine Chemistry* 177 (December): 134–42. https://doi.org/10.1016/j.marchem.2015.03.012.

Finstad, Anders G., Tom Andersen, Søren Larsen, Koji Tominaga, Stefan Blumentrath, Heleen A. de Wit, Hans Tømmervik, and Dag Olav Hessen. 2016. "From Greening to Browning: Catchment Vegetation Development and Reduced S-Deposition Promote Organic Carbon Load on Decadal Time Scales in Nordic Lakes." *Scientific Reports* 6 (1): 1–8. https://doi.org/10.1038/srep31944.

Fu, Hongbo, Raluca Ciuraru, Yoan Dupart, Monica Passananti, Liselotte Tinel, Stéphanie Rossignol, Sebastien Perrier, D. James Donaldson, Jianmin Chen, and Christian George. 2015. "Photosensitized Production of Atmospherically Reactive Organic Compounds at the Air/Aqueous Interface." *Journal of the American Chemical Society* 137 (26): 8348–51. https://doi.org/10.1021/jacs.5b04051.

Gouw, J. A. de, P. D. Goldan, C. Warneke, W. C. Kuster, J. M. Roberts, M. Marchewka, S. B. Bertman, A. A.P. Pszenny, and W. C. Keene. 2003. "Validation of Proton Transfer Reaction-Mass Spectrometry (PTR-MS) Measurements of Gas-Phase Organic Compounds in the Atmosphere during the New England Air Quality Study (NEAQS) in 2002." *Journal of Geophysical Research D: Atmospheres* 108 (21): 4682. https://doi.org/10.1029/2003jd003863.

Hansel, A., A. Jordan, R. Holzinger, P. Prazeller, W. Vogel, and W. Lindinger. 1995. "Proton Transfer Reaction Mass Spectrometry: On-Line Trace Gas Analysis at the Ppb Level." *International Journal of Mass Spectrometry and Ion Processes* 149–150 (C): 609–19. https://doi.org/10.1016/0168-1176(95)04294-U.

Harvey, George W., and Linden A. Burzell. 1972. “Simple Microlayer Method for Small Samples.” *Limnology and Oceanography* 17 (1): 156–57.

Ininbergs, Karolina, Guillaume Bay, Ulla Rasmussen, David A. Wardle, and Marie Charlotte Nilsson. 2011. “Composition and Diversity of NifH Genes of Nitrogen-Fixing Cyanobacteria Associated with Boreal Forest Feather Mosses.” *New Phytologist* 192 (2): 507–17. https://doi.org/10.1111/j.1469-8137.2011.03809.x.

Kattner, G., G. Gercken, and K. D. Hammer. 1983. “Development of Lipids during a Spring Plankton Bloom in the Northern North Sea. II. Dissolved Lipids and Fatty Acids.” *Marine Chemistry* 14 (2): 163–73. https://doi.org/10.1016/0304-4203(83)90039-7.

Kieber, Robert J., Linda H. Hydro, and Pamela J. Seaton. 1997. “Photooxidation of Triglycerides and Fatty Acids in Seawater: Implication toward the Formation of Marine Humic Substances.” *Limnology and Oceanography* 42 (6): 1454–62. https://doi.org/10.4319/lo.1997.42.6.1454.

Knulst, Johan C., Peter Backlund, Dag O. Hessen, Gunnhild Riise, and Anders Södergren. 1997. “Response of Surface Microlayers to Artificial Acid Precipitation in a Meso-Humic Lake in Norway.” *Water Research* 31 (9): 2177–86. https://doi.org/10.1016/S0043-1354(97)00061-4.

Mann, Marvin M., Andrew Hustrulid, and John T. Tate. 1940. “The Ionization and Dissociation of Water Vapor and Ammonia by Electron Impact.” *Physical Review* 58 (4): 340–47. https://doi.org/10.1103/PhysRev.58.340.

Martinez-Varela, Alícia, Gemma Casas, Benjamin Piña, Jordi Dachs, and Maria Vila-Costa. 2020. “Large Enrichment of Anthropogenic Organic Matter Degrading Bacteria in the Sea-Surface Microlayer at Coastal Livingston Island (Antarctica).” *Frontiers in Microbiology* 11 (September): 2153. https://doi.org/10.3389/fmicb.2020.571983.

Noregs vassdrags- og energidirektorat (NVE). 2020. “Innsjødatabase.” NVE Innsjødatabase. 2020. https://www.nve.no/karttjenester/kartdata/vassdragsdata/innsjodatabase/.

Peterson, Kirk A., Sotiris S. Xantheas, David A. Dixon, and Thom H. Dunning. 1998. “Predicting the Proton Affinities of H2O and NH3.” *Journal of Physical Chemistry A* 102 (14): 2449–54. https://doi.org/10.1021/jp971510r.

Rossignol, Stéphanie, Liselotte Tinel, Angelica Bianco, Monica Passananti, Marcello Brigante, D. James Donaldson, and Christian George. 2016. "Atmospheric Photochemistry at a Fatty Acid-Coated Air-Water Interface." *Science* 353 (6300): 699–702. https://doi.org/10.1126/science.aaf3617.

Schultz, Martin G., Sabine Schröder, Olga Lyapina, Owen R. Cooper, Ian Galbally, Irina Petropavlovskikh, Erika von Schneidemesser, et al. 2017. "Tropospheric Ozone Assessment Report: Database and Metrics Data of Global Surface Ozone Observations." *Elementa* 5 (January): 43. https://doi.org/10.1525/elementa.244.

Seco, Roger, Thomas Holst, Mikkel Sillesen Matzen, Andreas Westergaard-Nielsen, Tao Li, Tihomir Simin, Joachim Jansen, et al. 2020. "Volatile Organic Compound Fluxes in a Subarctic Peatland and Lake." *Atmospheric Chemistry and Physics* 20 (21): 13399–416. https://doi.org/10.5194/acp-20-13399-2020.

Thrane, Jan Erik, Dag O. Hessen, and Tom Andersen. 2014. "The Absorption of Light in Lakes: Negative Impact of Dissolved Organic Carbon on Primary Productivity." *Ecosystems* 17 (6): 1040–52. https://doi.org/10.1007/s10021-014-9776-2.

Tovar-Sánchez, Antonio, Enrique González-Ortegón, and Carlos M. Duarte. 2019. "Trace Metal Partitioning in the Top Meter of the Ocean." *Science of the Total Environment* 652 (February): 907–14. https://doi.org/10.1016/j.scitotenv.2018.10.315.

Tranvik, Lars J., John A. Downing, James B. Cotner, Steven A. Loiselle, Robert G. Striegl, Thomas J. Ballatore, Peter Dillon, et al. 2009. "Lakes and Reservoirs as Regulators of Carbon Cycling and Climate." *Limnology and Oceanography* 54 (6 PART 2): 2298–2314. https://doi.org/10.4319/lo.2009.54.6_part_2.2298.

Vuorio, Kristiina, Marko Järvinen, and Niina Kotamäki. 2020. "Phosphorus Thresholds for Bloom-Forming Cyanobacterial Taxa in Boreal Lakes." *Hydrobiologia* 847 (21): 4389–4400. https://doi.org/10.1007/s10750-019-04161-5.

Wurl, Oliver, Werner Ekau, William M. Landing, and Christopher J. Zappa. 2017. "Sea Surface Microlayer in a Changing Ocean - A Perspective." *Elementa*. University of California Press. https://doi.org/10.1525/elementa.228.

Zäncker, Birthe, Astrid Bracher, Rüdiger Röttgers, and Anja Engel. 2017. "Variations of the Organic Matter Composition in the Sea Surface Microlayer: A Comparison between Open

Ocean, Coastal, and Upwelling Sites off the Peruvian Coast." *Frontiers in Microbiology* 8 (DEC): 2369. https://doi.org/10.3389/fmicb.2017.02369.

Zhang, Zhengbin, Liansheng Liu, Chunying Liu, and Weijun Cai. 2003. "Studies on the Sea Surface Microlayer: II. The Layer of Sudden Change of Physical and Chemical Properties." *Journal of Colloid and Interface Science* 264 (1): 148–59. https://doi.org/10.1016/S0021-9797(03)00390-4.

Zhou, S., L. Gonzalez, A. Leithead, Z. Finewax, R. Thalman, A. Vlasenko, S. Vagle, et al. 2014. "Formation of Gas-Phase Carbonyls from Heterogeneous Oxidation of Polyunsaturated Fatty Acids at the Air-Water Interface and of the Sea Surface Microlayer." *Atmospheric Chemistry and Physics* 14 (3): 1371–84. https://doi.org/10.5194/acp-14-1371-2014.

Zhou, Xianliang, and Kenneth Mopper. 1997. "Photochemical Production of Low-Molecular-Weight Carbonyl Compounds in Seawater and Surface Microlayer and Their Air-Sea Exchange." *Marine Chemistry* 56 (3–4): 201–13. https://doi.org/10.1016/S0304-4203(96)00076-X.

Zhu, Tao, Thibault Scalvenzi, Nathalie Sassoon, Xuefeng Lu, and Muriel Gugger. 2018. "Terminal Olefin Profiles and Phylogenetic Analyses of Olefin Synthases of Diverse Cyanobacterial Species." *Applied and Environmental Microbiology* 84 (13). https://doi.org/10.1128/AEM.00425-18.

# Appendix

## A1. Supplementary sample information

Table 4. Sampling location information

| Lake | Elevation (m) | Lake surface area ($km^2$) | Catchment area ($km^2$) | Coordinates | |
|---|---|---|---|---|---|
| | | | | Latitude | Longitude |
| Tennungen | 298 | 0.28 | 8.6 | 60.352396 | 11.443084 |
| Sværsvann | 136 | 0.48 | 16 | 59.817789 | 10.888946 |
| Svartkulp | 372 | 0.0046 | 0.29 | 59.975509 | 10.737049 |
| Tjernsrudtjern | 61 | 0.011 | 0.65 | 59.921085 | 10.609357 |
| Sessvoldtjern | 200 | 0.018 | 1.3 | 60.250020 | 11.164780 |
| Årungen | 34 | 1.2 | 50 | 59.701097 | 10.739540 |
| Gjersjøen | 40 | 2.7 | 82 | 59.758267 | 10.781886 |
| Kolbotntjern | 95 | 0.29 | 3.1 | 59.809404 | 10.800307 |
| Østensjøvann | 107 | 0.33 | 12 | 59.881344 | 10.831921 |
| Lutvann | 205 | 0.42 | 1.7 | 59.920002 | 10.877728 |